

---

This manuscript is a preprint and has not undergone peer-review. Please note that subsequent versions of this manuscript may have different content. If accepted, the final version of this manuscript will be available via the 'Peer-reviewed Publication DOI' link on the right-hand side of this webpage. Please feel free to contact any of the authors, we welcome feedback.

---

## **Basin and depositional control on the initiation and development of fluid-escape pipes in the Canterbury Basin, New Zealand.**

Omosanya, Kamaldeen O. Leif <sup>1,2\*</sup>, Micallef Aaron<sup>2</sup>, Harishidayat Dicky <sup>3</sup>

<sup>1</sup>Oasisgeokonsult, 7052, Trondheim.

<sup>2</sup>Department of Geosciences, University of Malta, Msida.

<sup>3</sup>College of Petroleum Engineering and Geosciences,  
King Fahd University of Petroleum and Minerals, Dhahran.

### **ORCID Numbers**

Omosanya, Kamaldeen O.L      0000-0001-8959-2329

Micallef Aaron                      0000-0002-9330-0648

Harishidayat D                      0000-0003-3729-2441

Corresponding author email: [kamal.omosanya@oasisgeokonsult.com](mailto:kamal.omosanya@oasisgeokonsult.com)

Twitter of Kamaldeen Omosanya @extratectonics

Twitter of Dicky Harishidayat @thearishidayat

### **Abstract**

The influence of basin and depositional context on the formation and growth of fluid escape pipes in sedimentary basins is not fully understood. While seismic reflection data is commonly used to study these structures, direct observation and sampling of field analogues of pipes and their related structures are rare. In this study, we investigate the evolution of meter-tall fluid escape pipes (100-800 m) in the Canterbury Basin, New Zealand, using open source seismic and borehole data. Our analysis includes seismic interpretation of 19 unconformities within the Neogene-Quaternary successions, characterization of pipes and fluid-related anomalies in the subsurface, modelling of the shale volume (V<sub>sh</sub>), lithology characterization, 3D static modelling, and seismic inversion. We identify thirty-one vertical to sub-vertical pipes with three parts consisting of top, main conduit/stem, and root zone on seismic profiles. Our results suggest that lithology plays a crucial role in the initiation and modulation of pipe structures in the Canterbury Basin, with pipes mostly formed post Tarantian (0.113 Ma) and truncated at the U19 unconformity. Furthermore, vertical fluid migration from overpressured units, such as the tops of contourite mounds, was observed in the pipes. Our findings provide new insights into the subsurface fluid flow and sedimentary architecture of the Canterbury Basin and have wider implications for other passive continental margins with similar characteristics.

**Keywords:** lithology, geomorphology, fluid escape pipes, contourite, Canterbury Basin, seismic reflection, borehole data.

## 1. Introduction

Fluid migration from the subsurface to the seabed along continental margins is often aided by vertical to sub-vertical structures known as fluid escape pipes (Andresen, 2012; Berndt, 2005; Maestrelli et al., 2017; Paganoni et al., 2018). In several basins, these structures are evidence of past vertical fluid migration (Chen et al., 2021a; Huuse et al., 2010; Moss and Cartwright, 2010), seal bypass systems (Cartwright et al., 2007; Oppo et al., 2021), and any possible compromise of CO<sub>2</sub> storage reservoirs. Pipes may be an important component of many hydrologic systems, allowing for the transmission of fluids under overpressure across subsurface formations (Böttner et al., 2021; Oppo et al., 2021). In environments where gas hydrates are present, the potential for pipes to connect the underlying free gas reservoir and the atmosphere is of particular concern for greenhouse gas (GHG) mitigation efforts (Berndt, 2005; Elger et al., 2018).

Seismic reflection data has proven to be an invaluable tool for understanding the anatomy and dimensionalities of fluid-escape pipes. Such pipes are typically manifested as highly localized vertical to sub-vertical pathways of low- or high-amplitude seismic anomalies. On seismic reflection data, pipe structures are characterized by columnar zones of disrupted reflection continuity, along with associated amplitude and velocity anomalies, acoustic blanking at the base of the pipes, scattering, attenuation, and transmission artifacts (Berndt et al., 2003; Løseth et al., 2009, 2011; Moss and Cartwright, 2010; Paganoni et al., 2018). Pockmarks are typically observed at the top of pipe structures, while their bases can present diffused and low amplitude reflections (Leduc et al., 2013), or complex and variably shaped high amplitude magmatic sills in magma-rich continental margins (Omosanya et al., 2020). Pipe-related structures are rarely drilled, making seismic reflection data the primary source of information for characterizing their internal lithological make up. Though direct observation and sampling of field analogues of pipes and their related structures can provide insight into physical structure, geometry, and properties, such analogues are scarce. These have been documented in Norway and Scotland (Grove, 2013; Planke et al., 2022; Svensen et al., 2006), Utah, USA (Hurst et al., 2011; Huuse et al., 2005), Varna, Bulgaria (Böttner et al., 2021), Western Desert, Egypt (Mazzini et al., 2019), the Karoo Basin, South Africa (Svensen et al., 2006), the Siberian Traps, Russia (Neumann et al., 2017), Antarctica (Elliot and Grimes, 2011), and Java (Manton et al., 2022).

The external and internal composition of pipes in sedimentary basins therefore are still poorly understood, and the impact of lithology, intra-basinal and geomorphologic structures on their formation is often debated (Cartwright and Santamarina, 2015; Omosanya et al., 2020). Pipes are largely documented from Neogene marine sedimentary successions, typically occurring at depths up to one kilometer, and consisting of claystones and sandstone units. To date, there has been no report of pipes crossing thick (>100s of meters) sandstone or limestone units, apart from those associated with the dissolution of limestone units (Bertoni and Cartwright, 2005; McDonnell et al., 2007). In parallel, seismic reflection data shows that hydraulic fracturing is the most common formation process for fluid pipes in the subsurface (Foschi et al., 2014). Other processes, such as erosive fluidization, capillary invasion, localized volume loss collapse, and syn-sedimentary flow localization, are reported less often (Cartwright and Santamarina, 2015).

In addition to the physical and internal control on pipe formation, more recent investigations have demonstrated the importance of geobodies and geomorphological structures, such as salt diapirs, mass-transport complexes (MTCs), and contourites, in the initiation, modulation, and growth of fluid pipes (Oppo et al., 2021; Browne et al., 2020; Kirkham et al., 2019; Ruge et al., 2021; Wu et al., 2021). Contrary to the traditional notion that fluid pipes form from the structural crests of large anticlines (Cartwright et al., 2021a) or lateral pressure transfer zones (Stump and Flemings 2000; Flemings et al. 2003), recent studies have revealed the presence of fluid pipes in several other settings. These include synclines, topographic lows, and softly inclined layers in the absence of structural impediments (Cartwright and Santamarina 2015), as well as in areas where geomorphologic structures are dominant (Omosanya et al., 2020).

In this study, we explore the evolution of meters-tall pipes in the Canterbury Basin (CB), their formation mechanism, and investigate how lithology and geomorphologic structures influence their initiation and

growth (Figure 1). This basin preserves a unique record of high-frequency (0.1–0.5 Ma periods) depositional sequences (Browne and Naish, 2003; Lu and Fulthorpe, 2004), offering an opportunity to examine how lithologic and geomorphologic structures can affect pipe formation and healing. In the Canterbury Basin, nineteen sequence-bounding unconformities from the Middle Miocene to Holocene have been identified and dated, based on geophysical, biostratigraphic and geochemical data (Fulthorpe and Carter, 1991; Lu and Fulthorpe, 2004; McHugh et al., 2018). These unconformities separate different strata and lithologic facies, and reflect the influence of bottom currents, glacial-interglacial cycles, and associated eustatic sea-level changes. As a result, this is an excellent opportunity to investigate the relationship between bottom currents and the temporal-spatial growth of pipes. Importantly, the results of this study imply that lithology is important in the initiation and modulation of pipe structures in the Canterbury Basin, which may be relevant to other passive continental margins with comparable characteristics.

## 2. Geological setting

The Canterbury Basin of the South Island of New Zealand lies on the eastern margin of the rapidly rising Southern Alps, and encompasses the onshore Canterbury Plains, the Canterbury Bight shelf, and the offshore continental slope (Figure 1). The basin is delimited to the west by the Southern Alps, and to the north by the Hope Fault or the Hurunui High, a west-east trending structural feature that formed during Cretaceous and Paleogene times, dividing the Canterbury and East Coast Basins (Schiøler et al., 2011). The eastern boundary of the CB is poorly differentiated, but merges with the Bounty Trough at ca. 174°E longitude while the southern part of the basin is connected to the Great South Basin (Schiøler et al., 2011). In terms of physiography, the offshore part of the CB covers an area of about 50,000 km<sup>2</sup> and includes a shelf that is broad and about 100 km wide (Figure 1). Modern water depths in the offshore basin can reach ca. 1.5 km and with ca. 8 km of Cretaceous to Quaternary rift and sag basin sedimentary fill (Field and Browne, 1989). The offshore part of the Canterbury Basin has been relatively stable since rifting, despite being located ca. 200 km from the Alpine Fault (Browne and Field, 1988). The Canterbury Bight comprises a continental shelf that is about 180 km long and up to 95 km wide, with a shelf gradient of 0.09° and a maximum depth of 140 to 150 m (Browne and Naish, 2003).

The Canterbury Basin has experienced four distinct phases of tectono-sedimentary evolution since the Permian-Mid Cretaceous period. The first phase was characterized by convergence and passive margin formation. This was followed by rifting and breakup of Gondwana during the Late Cretaceous, which initiated passive subsidence and northwest-directed transgression that continued into the Paleogene. The last phase is characterized by progressive uplift and erosion of the Southern Alps (Bradshaw, 1989; Kamp, 1986; King, 2000; Molnar et al., 1975; Sutherland and Browne, 2003). The earliest tectonic activity of the Canterbury Basin dates to the Permian to Early Cretaceous convergent margin stage, with large volumes of sedimentary rocks of the Torlesse Terrane being deposited (Field and Browne, 1989). The oldest basin architecture reflects an accretionary convergent margin setting (Sutherland and Browne, 2003) consequent to the collision between the Pacific and the Phoenix plates, which ended in the Early Cretaceous (Bradshaw, 1989). This collision was followed by the initiation of separation of New Zealand from Antarctica and Australia in the mid-Cretaceous (Molnar et al., 1975). Spreading along the Pacific-Phoenix ridge, the initial spreading center in the Tasman Sea and South of Australia, resulted in extensional tectonics in New Zealand causing the eastern margin of the South Island of New Zealand to rift from the Marie Byrd Land in West Antarctica at ca. 80 Ma (Bradshaw, 1989; Molnar et al., 1975).

In the mid-Cretaceous, New Zealand, Antarctica, and Australia began to separate in response to the break-up of Gondwana (Carter and Norris, 1976; King, 2000). The New Zealand block experienced a period of relative tectonic stability with slow subsidence in the central part of the Canterbury Basin and continued to drift away from Antarctica until the Late Eocene (Browne and Field, 1988). In the Late Eocene, the sub-continent was exposed to oblique separation and deformation, but this deformation did not affect the Canterbury Basin (Molnar et al., 1975). The eastern margin of the South Island of New Zealand, including the Canterbury Basin remained a passive margin until the Late Eocene (ca. 23 Ma) when the Alpine fault was formed (King, 2000). The Alpine fault is a dextral strike-slip fault (ca. 500 km displacement) that forms the boundary between the Australian and the Pacific plates (King, 2000;

Wood and Stagpoole, 2007). Subduction along the North Island of New Zealand with oblique convergence and northwest-oriented oblique subduction of the South Island have resulted in transpressive movement on the Alpine Fault since ca. 23 Ma (Norris and Cooper, 2001; Wood and Stagpoole, 2007). Oblique convergence across these plate boundaries resulted in deformation along the Alpine Fault, and uplift and erosion of the Southern Alps. At ca. 10 Ma, deformation along the Alpine fault accelerated resulting in high rates clastic influx to the offshore Canterbury Basin since Late Miocene (Sutherland et al., 2007). Terrigenous sediment had begun accumulating offshore Canterbury Basin by perhaps as early as 15 Ma (Fulthorpe and Carter, 1991) while timing of the Southern Alps uplift is put at either ca. 8 to 5 Ma (Tippett and Kamp, 1993) or ca. 10 to 8 Ma (Carter and Norris, 1976; Norris et al., 1978).

Neogene sediments in the Canterbury Basin are associated with the development of the modern plate boundary, transpressive motion at the Alpine Fault, and uplift and erosion on the South Island (Carter, 1988). Large, modern, coarse-grained, braided rivers from north to south, with sources in the Southern Alps, have shed significant volumes of sediment (50,000 km<sup>3</sup>) onto the margin since 5 Ma (Browne and Naish, 2003). The Neogene Otakou Group are siliciclastic sediments, composed predominantly of terrigenous siltstone and silty mudstone, with lesser amounts of fine-grained to very fine grained sandstone and mudstone (Hawkes and Mound, 1984; Wilson, 1985). Recent offshore coring by Expedition 317 at Sites U1351, U1352, U1353 and U1352 showed that the Otakou Group also contains marly calcareous beds (Fulthorpe et al., 2011). In the Miocene to Recent succession of the Canterbury Basin (Figures 2-4), nineteen regional sequence boundaries and 14 local unconformities are present (Lu and Fulthorpe, 2004). This is in addition to large sediment drifts that developed within the Otakou Group since the Early Miocene (Fulthorpe et al., 1996; Fulthorpe and Carter, 1991). At least eleven large elongate drifts formed within the Otakou Group near the slope toe and aggraded to upper-slope water depths (Lu et al., 2003). These drifts are precursors of colder and fresher Subantarctic Front (SAF) and the Southland Current systems (Fulthorpe et al., 1996; Lu et al., 2003).

### **3. Data and methods**

#### *3.1 Seismic and Borehole Data*

The datasets used for this study include open source two-dimensional seismic reflection and borehole datasets from the Canterbury Basin. The seismic data is a high quality MCS seismic survey acquired by R/V Maurice Ewing (cruise EW0001) in January 2000. The EW0001 seismic survey consists of 57 2-D seismic profiles (ca. 3250 line-km in length) that jointly covers a surface area of ca. 4840 km<sup>2</sup> on the middle to outer shelf and slope in water depths of 40 to 1100 m. Line spacings for the lines are ca. 2 km in the dip direction (perpendicular to the coastline) and 2 to 5.5 km in the strike direction (parallel to the present-day coast). The EW data were acquired with a seismic source with two generator-injector (GI) air guns (45/45 in<sup>3</sup>), and streamers that were deployed with 12.5 m groups in 96- and 120-channel configurations. The GI guns provided a high-frequency source with frequencies of 100 to 500 Hz. Hence, a velocity of ca. 1470 m/s below the seafloor gives vertical resolutions of ca. 2.45 - 4 m. Recording lengths and vertical sampling interval for all the EW0001 seismic profiles are 3 seconds and 1 ms, respectively.

Borehole data available in the Canterbury Basin include five exploration wells (Galleon-1, Endeavour-1, Clipper-1, Resolution-1, and Cutter-1) and five IODP Site (Figures 2-4). Lithological characterization, synthetic seismogram generation, seismic-to-well ties, petrophysical characterization, and Vsh modelling were conducted in the EW0001 grid using Clipper and IODP Site 1119. The synthetic seismograms generated from the Clipper well-1 and IODP 1119 data were found to be in excellent agreement with the seismic reflection events on the EW0001-17 and EW0001-28 seismic profiles, respectively. Moreover, the checkshot information from the Clipper-1 well and velocity information from the ODP 1119 were in satisfactory agreement, providing a reliable basis for the development of a time-depth (T-D) relationship, which was then used for seismic-tie of boreholes U1351, U1352 U1353 and U1354 to the EW0001-66 and EW0001-60 seismic profiles (Figures 3 and 4). Core samples acquired during IODP Expedition 317 (Sites U1351, U1352 U1353 and U1354) also provided additional lithological information.

### 3.2 Horizon interpretation and characterization of fluid-related anomalies and pipes.

The seismic interpretation of the nineteen unconformities was based on established sequence stratigraphic methods, such as the interpretation of seismic internal architecture, seismic facies, and lap geometries (Vail et al., 1977). The sequence boundaries were identified by a downward shift in the position of coastal onlap reflections/prograding shorelines and erosional truncations associated with subaerial erosion of older and underlying sequences on the paleo shelf. Thickness maps for unconformities U19-U16 were converted from the time domain to depth using a conservative average velocity of 1470m/s. This velocity information was obtained from the Clipper-1 borehole and the IODP 1119 site (Figure 2). For depth conversion of the TWTT thickness maps (isochore/vertical thickness), angle of dip was calculated for each interval and then used to estimate the isopach (stratigraphic true thickness) maps. Hence, the final isopach map is the product of the TWTT thickness maps, cosine (angle of dip) and average velocity of 1470 m/s.

Furthermore, columnar, vertical and sub-vertical zones with disturbed reflection continuity, as well as related amplitude anomalies, acoustic blanking, reflection scattering, and attenuation define pipe structures on seismic reflection profiles (Berndt et al., 2003; Løseth et al., 2009a, 2011a; Moss and Cartwright, 2010; Paganoni et al., 2018). On the other hand, seismic anomalies related to fluid leakage in the subsurface are defined by abrupt increase in seismic amplitude that contrasts with background amplitude value (Alves et al., 2015; Mohammedyasin et al., 2016). They are localized brightening of negative amplitude reflections. Since an increase in acoustic impedance with depth is a positive peak at the seabed reflection, anomalies with reversed polarity relative to the seabed are considered to be fluid-related i.e., seepage of oil, gas (methane), or water (Alves et al., 2015; Mohammedyasin et al., 2016). In addition to the identification of these anomalies on seismic profiles, envelope seismic attribute was also used for their characterization. The envelope attribute is the total instantaneous energy of the analytic signal (the complex trace), and it is independent of the phase. The envelope attribute is also known as 'Instantaneous Amplitude', 'Magnitude' or 'Reflection strength (Taner, 2001). The envelope seismic attribute is useful for detecting bright spots caused by gas accumulations, detecting major lithological changes that are caused by strong energy reflections, and sequence boundaries (Ismail et al., 2020). In this work, the envelope provided insights into the spatial extent of enhanced reflections and flat negative seismic amplitude anomalies.

### 3.3 Shaliness Index as proxy for lithology and seismic inversion of Vsh (Tertiary)

Gamma ray log is the only wireline log that is consistently available for all the wellbores and IODP Expedition 317 sites in the study area. Hence, the shale volume (Vsh) was estimated from the gamma log and further used for lithology characterization, 3D static modelling and seismic inversion. To estimate the Vsh, the IGR was first calculated as shown in Eq. 1. Although, the IGR provides a shaliness index, it can often yield an overestimation of rock's volume of shale (specially for shallow, young reservoirs), producing an overall pessimistic scenario of the reservoir quality. To overcome this challenge, the Larionov Vsh index for Paleogene rocks (Szabó, 2011), commonly referred to as the Vsh (Tertiary) in Eq. 2 was used. For all the wells, the shale and sand baseline represent both GRMax and GRmin were estimated as 130 API and 10 API, respectively.

$$\text{IGR} = \frac{\text{GRLog} - \text{GRMin}}{\text{GRMax} - \text{GRMin}} \quad \text{Eq. 1}$$

$$\text{Vsh (Tertiary)} = 0.083 * (2^{(3.7 * \text{IGR})} - 1) \quad \text{Eq. 2}$$

Seismic inversion of the seismic profiles was based on the calculated Vsh Tertiary data from Eq 2. The Vsh Tertiary cut-off, based on interpretation of lithology from core data and Vsh Tertiary log are as follows; 0% - 0.10% (Sand), 0.10% - 0.15% (Sandy mud), 0.16% - 0.50% (Muddy sand), 0.50% - 1.00% (Mud). Subsequently, the Vsh Tertiary property logs were extrapolated along the 2D seismic reflection data using the interpreted seismic horizons with default weighting inversely proportional to the square of the distance from the well. Moreover, the Vsh (Tertiary) seismic inversion used a deterministic approach on the 2D seismic reflection data, with colored inversion seismic reflection data

combining the frequency spectra of Vsh (Tertiary) logs with the computed average amplitude spectrum of the input seismic reflection data, resulting in better alignment with Vsh logs data (Veeken and Da Silva, 2004; Kemper and Gunning, 2014).

### *3.4 3D lithologic model of the Neogene-Quaternary succession based on Vsh*

A suite of 3D lithologic models of the Neogene-Quaternary succession of the Canterbury Bight were created based on the Vsh (Tertiary). These models include the present day (Seabed to U9), Tarantian (U19-U9), Upper Chibanian (U18-U9), Chibanian (U17-U9) and Calabrian (U16-U9) formations, dated as 0.113, 0.252-0.277, 0.74 and 1.05 Ma, respectively (Figure 2). All the models were built to cover the three main boreholes on the paleoshelves using a grid size of 50 meters in X and Y directions and a total number of grid cells of 1762 x 1701 (3,007,734). A finer grid block could not be used as it poses an enormous number of computational resources. The static modelling process was divided into zone modelling (making of horizons, zones, and layers), upscaling, and property modelling. For the present day model, horizons for the seabed and the U9 were used as the top and base surfaces, while U19, U18, U17 and U16 were the intermediate units. Since most of these horizons are relatively flat on the paleoshelves, the horizons were conditioned as being conformable from top to base. Five zones were further made from the top to base horizon. These include the Zone 1 (Seabed-U19), Zone 2 (U19-U18), Zone 3 (U18-U17), Zone 4 (U17-U16) and Zone 5 (U16-U9). Internal stratification of these zones was modelled as 2 layers for Zone 1 and 3 layers for Zones 2 to 5.

After the model set-up, the calculated Vsh (Tertiary) from the wells were upscaled using input from U1353, U1354 and U1351. The upscaling method involves coarsening of the grid cells and the averaging of VSh across the wells. The arithmetic averaging method was adopted as it is suitable for properties such as porosity, saturation and net/gross (fractions) because these are additive variables. To populate the zones and grids with the upscaled VSh values, the Sequential Gaussian Simulation (SGS) approach was used. Total sill value of 1.0, Nugget of 0.001 and spherical Variogram were used. Based on the trend of the coastline, an azimuth of 45 degrees was calculated and used for the property modelling. The same procedure was repeated for the other four models, using different upper and base units. The upper units used were Horizons U19, U18, U17, and U16, respectively, while the base unit used was Horizon U9 (top of strata older than 3.72 Ma).

## **4. Results**

### **4.1 Neogene-Quaternary Seismic Stratigraphy of the study area**

Of the nineteen unconformities interpreted on the seismic profile, eight (8) are key to understand the evolution and control on the formation fluid-escape pipes in the study area (Figures 2-7). The eight unconformities are further divided into four Pleistocene unconformities (1.05 Ma to 0.113 Ma) sequence boundaries where the tops of most pipes are found. Based on nannofossils and foraminifera assemblages (Figure 2) of core samples in the ODP Site 1119 well (Carter et al., 2004; Lu and Fulthorpe, 2004), these four horizons are dated Calabrian (1.05 Ma), Chibanian (0.74 Ma), Upper Chibanian (0.252-0.277 Ma) and Tarantian (0.113 Ma). The interpreted horizons are the same as unconformities U16, U17, U18 and U19 in Lu and Fulthorpe (2004). The last four horizons or unconformities are key to finding the root zones of the pipes. They are U9 (3.72 Ma), U4 (12.4 Ma), U1 (>15.1 Ma) and U0 (>15.1 Ma).

On seismic profiles, U19 to U16 are characterized by continuous, flat to undulated, and low to moderate amplitude reflections on the western part of the EW0001 survey (Figures 3 and 4). On the western part of the survey, the horizons transit into sigmoid and oblique reflections or simply put clinofolds (Figure 4). Importantly, all the horizons have downlap reflections above them and truncation below. And as such are architecturally defined by unique shelf onlap, shelf channel incisions, truncation of underlying reflections near paleo-shelf edges, and changes in internal reflection architecture (Figure 4). Horizons, U19 to U16 are therefore defined as sequence boundaries. Moreover, the change in reflection pattern from the west to the east of the EW0001 survey signifies changing depositional regime or environments from paleo shelves to continental slopes, and then deep-water environments. A drastic change in depositional regime from the paleoshelf to the slope is marked by the shelf break, which geometrically are also the topset-slope rollover points (Figure 3). The topset of the shelf-margin clinofolds is the

morphological shelf; the upper rollover of the clinoforms is the “shelf–slope break”, and “slope” is the deeper-water surface below (Johannessen and Steel, 2005; Safronova et al., 2014).

The interpreted paleoshelves in the study area are generally unfaulted and almost flat with relatively constant thickness for the sequences bounded by U19 to U16 (Figure 5). Stratigraphic thicknesses can reach ca. 192 m from the seabed to U19, ca. 217 m for the U19 sequence, ca. 138 m for U18, ca. 174 m for U17, and ca. 593 m for U16 to U9 (Figure 5). The thicknesses increase considerably from the shelf-break points to the paleo slope. It should be noted that interpretation of U19 to U16 could not be extended further into the deep waters as the horizon interpretation often extends into areas covered by younger drifts (Figure 3). Hence, the estimated thicknesses in the slope areas are approximate values. Nevertheless, by mapping the trajectory of the shelf break points (Figures 5a-5d), it is noted that there is a southeast shift in depositional regimes along the Canterbury Basin since 3.72 Ma till Recent. The clinoforms associated with U19-U16 characteristically show a general ascending regressive trajectory showing continuous rise in sea-level since 3.72 Ma (Figure 4). Ascending shelf-edge trajectories are associated with ascending regressive shorelines with sands having a higher potential to accumulate on the slope rather than on the basin floor (Johannessen and Steel, 2005). Ascending trajectories will result in a sigmoidal seismic pattern and long-term rise in relative sea level (Johannessen and Steel, 2005; Omosanya et al., 2016).

The older horizons beneath U16 are slightly different in terms of their geometries and seismic facies (Figure 3), although U9 and U4 show similar topset, upper rollover, and slope facies (Figure 3b). However, their internal reflections are flatter compared to the Pleistocene-Quaternary sequences possibly owing to their depth of occurrence or compaction (Figures 3 and 4). On seismic profiles, reflections capped by U9 and U4 are continuous, low to moderate amplitude, oblique and often downlap onto the underlying sequence boundaries and truncating towards the west underneath both U9 and U4 (Figures 3 and 4). In comparison to the younger sequences, the eastern parts of U9 and U4 are cut by drifts of various geometries and, on occasion, by moat-related canyons. These canyons are surrounded by drift platforms and have vertical stacks of V-shaped reflections interpreted as contourite moats. (e.g., Figure 3). There is no discernible shelf-slope break after U4 down to the depth where U0 is interpreted. However, U- and V-shaped canyons associated with Miocene drifts are observed. These drifts are most dominant in the central part of the study area (Figure 3). U0 and U1 are the deepest horizons and relict of the main tectonic events that affected the area. On seismic profiles, both U0 and U1 are continuous and high amplitude reflections, which are intersected by normal faults towards the eastern part of the survey (Figure 3). It is possible that some of these faults are inverted.

#### **4.2 Fluid escape pipes and bright spots in the Neogene -Quaternary succession.**

The 31 pipes interpreted in the area are vertical to sub-vertical and upward widening structures on seismic profiles (Figures 6-9). The pipes can reach a height of about 1099.92 ms TWTT (808 m, using a constant velocity of 1470 m/s) while the shortest pipe in the study area is about 149.49 ms TWTT or 110 m tall (Figure 10a). Structurally, the pipes have three parts consisting of top, main conduit/stem, and root zone. Most of the pipes root zones are inferred below unconformity U16, where moat-related canyons, sediment drifts and drift platform are predominant (Figures 7a, 8b and 9a). Internally, the pipes are typified by low amplitude and distorted reflections (Figures 6-9). The low amplitude reflection of the pipes contrasts markedly with those of the surrounding or host-rock strata, and characteristically represent discontinuity of the surrounding reflections, weak reflection amplitudes, and disturbances in the seismic response (Figure 8b). Close to the inferred root zones, the pipes usually show dimmed reflections and more transparent reflection close to the tops. On the flanks of the pipes, faults (e.g., Figure 7) or high amplitude reflection can be present at intermediate levels e.g., Figure 8d.

In contrast to the root zones, the tops or upper limits of the pipes are mostly restricted to the U19 level (Figures 10b and 10c). At these tops, the pipe has a flat-crater shape (e.g., Figures 7a and 7c) or cone-shape (Figures 8 and 9). Additionally, negative high amplitude anomalies (NHAA) or bright spots indicative of accumulated fluids are often found (e.g., Figures 7 and 8a). Apart from the NHAA, flat and enhanced reflections can be present or conjoined with the pipe's top (e.g., Figure 9). These anomalies are generally mildly faulted and connected to underlying anomalies by small faults (Figures

9b-9d). In the study area, enhanced reflections are often flanked by pipes suggesting a connection between vertical and lateral plumbing units (Figure 8b). Their similarities with the seabed reflection on the envelope profiles might suggest they are tuning thickness reflections (Sheriff and Geldart, 1995) related to lateral stacking of thin and coarse-grained strata rather than anomalies related to fluid seepage.

Other bright spots away from the pipes in the study area are discrete but dispersed bright spots that are common along the paleo shelf break (Figure 8d). These anomalies can include hard kicks i.e., those with similar polarity as the seabed reflections or negative high amplitude anomalies (soft kicks). Pipes are sometimes found in association with dispersed hard and soft kick anomalies along the paleo shelf break (Figure 8d). The presence of negative high amplitude anomalies along the paleo shelf break enabled the identification of two NHAA zones in the study area (Figure 6). Zone 1 on the paleo shelf, where the NHAA interact with tall pipes, some of which extend down to deeper drift platforms, as shown in Figure 8d. In Zone 2, the NHAA are found in the proximity of short pipes that are mostly rooted within strata bounded by U19- U16. NHAA anomalies at the U19 level may indicate enhanced and intermittent fluid infiltration into a permeable subsurface reservoir (Hustoft et al., 2007).

#### **4.4 Three dimensional (3D) Vsh model of the paleoshelves**

Based on the analyses of the modelled VSh from the Gamma ray log (Figure 11), the seismic profiles in Figures 6 to 8 were inverted with the VSh values (Figure 12) and later used to build 3D lithology model of the paleoshelves on the Canterbury Basin (Figure 13). The inverted seismic profiles show that the strata beneath U19 are mostly a mix of low to intermediate Vsh values, i.e., heterogeneous mixtures of siliciclastic sediments dominated by mud, while the root zones and drift sediments are associated with intercalation of very muddy sediment to sediments with low sand content.. In parallel, the 3D models revealed that the study area can be characterized into three main lithologic domains (Figures 13). These are areas with (a) low sand potential i.e., areas with VSh of greater 20 % (b) intermediate sand potential, are areas with dispersed Vsh values overlapping between Vsh values of 10 to 20%, and (c) high sand potential, i.e., areas with VSh values of less than 10% (Figures 13).

For the present day model (Figure 13a), areas to the east of U1354 are modelled as areas with low sand potential while high sand potential areas are modelled close to U1354 and U1353. Strikingly, the upper 110 m of both boreholes were interpreted to consist of variety of sand, muddy sand and sandy mud in Figure 10. Another area with high sand potential is modelled at the NE part of the study area (Figure 13a). For the top Tarantian surface (U19), the model revealed mainly two lithologic domains (Figure 13b). An area with intermediate sand potential occur from north to south and around U1351, U1354 and U1353 (Figure 13b). This area is surrounded by areas of low sand potential. The highest sand potential is predicted to the south of U1354 for top Upper Chibanian while other areas are characterized by low to intermediate sand potential (Figure 13c). As for the Chibanian and Latest Calabrian, the areas with high sand potential are on the paleo slope and the central area to the SE paleo slope areas (Figures 13d and 13e), respectively. For the latest Calabrian, low sand potentials are predicted to SW and the northern part of the Canterbury Basin (Figure 13e). On the contrary, low sand potential are noted mainly at the central part of the study area to the western at the Chibanian (0.74 Ma) level (Figure 13d).

## **5. Discussion**

### *5.1 Initiation and evolution of pipes in the Canterbury Basin.*

Although seismic reflection data can be used to identify the tops and base zones of pipes, absolute dating cannot be guaranteed due to resolution, processing, and velocity problems (Yilmaz, 2001). On seismic reflection data, structures and stratigraphy are better defined at shallow depths than at greater depths (Omosanya et al., 2021). Nevertheless, the position of pipe tops and root zones can still provide information on the relative timeline of their initiation and growth. Pipes rooted at various stratigraphic levels, for example, suggest multiple fluid sources (Ruge et al., 2021) while those terminating at surface pockmarks imply a connection between the pipe and the pockmark, often via methane migration from the subsurface (Judd and Hovland, 2007). Cartwright and Santamarina (2015) discovered that pipes, which end at buried pockmarks, fed several vertically stacked paleo pockmarks. This suggests episodic activity in the formation of pipes. Additionally, pipes may terminate in a set of vertically stacked

amplitude anomalies above the primary location of seismic disruption. This may be due to a prolonged low flux flow regime that persisted after the formation of pipes. On the other hand, Van Rensbergen et al. (2007) observed that pipes may abruptly end at a specific subsurface horizon without any paleo-pockmark structure. This horizon could act as a barrier to the upward growth of pipes due to sediment variability in the shallow subsurface.

In the study area, one striking feature of the mapped pipes is that they are seismically uniform from the inferred root zones to their tops. The reflections within the pipes are transparent, distorted, or down-warped, signifying that they formed after the host-rock layers were deposited (Figures 7-9). Thus, the timing of pipe initiation and development is placed at post Tarantian (0.113 Ma) after the formation of the U19 unconformity. Moreover, most pipe tops prevail at the U19 level. Other proof for pipes reaching the present seabed was discovered (e.g., Figure 8), as well as some bright spots or enhanced reflections connecting with pipes between the U19 and the seabed reflection. Enhanced reflections close to the pipes are evidence for along-bedding or lateral migration of gas from areas of acoustic turbidity (Judd and Hovland, 2007; Schroot and Schüttenhelm, 2003). Enhanced reflections usually occur where fine grained sediments are interbedded with layers of coarse and permeable sediments. Hence, gas voids in the finer sediments causes acoustic turbidity while the gas bubbles within the coarser sediments or gas reservoir causes scattering of seismic wavelets and brightening of the negative amplitude (Anderson and Hampton, 1980; Hovland and Judd, 1988). However, due to a lack of data, the age of the seabed from this study could not be conclusively proven. Therefore, multiple phases of fluid seepage and pipe formation up until the Recent times in the study area cannot be ruled out.

### *5.2 Sources and types of fluids*

We propose that the other pipes with tops at older stratigraphic levels such as U18 and U9 also formed post Tarantian (0.113 Ma) based on the general lack of distinct syn-kinematic strata within them. Their termination at these levels (Figure 10c) could be attributed to sediment variability or inversion of permeability (Berndt et al., 2012; Van Rensbergen et al., 2007). Such that their growth was impeded by the presence of impermeable sediments at those levels, which restricted further vertical migration of the fluids. Similarly, for the most pipes truncated at U19, there are no distinct pockmarks or craters, but are instead conjoined with other anomalies or bright spots (Figures 8f and 9a). This concatenation of the pipe tops with other fluid structures or anomalies shows evidence for interactions between lateral and vertical fluid conduits, suggesting changes in sediment composition near the pipe tops and the presence of permeable intervals that aided lateral migration of fluid from the pipes. Moreover, Micallef et al. (2020) already showed that Pleistocene-Quaternary sequences between unconformities U16 to U19 have a potential to host groundwater aquifers in gravels to depths of approximately 150 m below the present-day seafloor.

On the source and types of fluids being leaked through the pipes, the spatial and temporal spread of the root zones shows that the source of fluids leaking through the pipes is multi-faceted, with seepage from multiple stratigraphic levels below the seabed. Predominantly, the root zones were found below U16, above U4, and above U9 (Figure 10b). For those above U4, they are associated with sediment drifts, occurring along the flanks of moat canyons, and on the crest of contouritic mounds (Figures 8d-8f). In map view, these latter pipes appear to be preferentially sited along the trends of large and underlying seismically resolvable sediment drifts (Figure 6). Carter et al. (2004) and Lu and Fulthorpe (2004) mapped these sediment drifts and show that they have a NE-SW orientation and are precursors of colder and fresher Subantarctic Front (SAF) and Southland bottom current systems (Fulthorpe et al., 1996; Lu et al., 2003). A corollary of having the fluids sourced from different intervals or units is that the fluid composition may also vary. For example, pore fluids or biogenic gas may be present in shallower depths (e.g. U18 to U16), while thermogenic hydrocarbons, mud slurry, or water expelled during compaction may be present in deeper stratigraphic levels (see above and below U4). This highlights the importance of considering the stratigraphic context and root zones when analyzing fluid composition from pipes (Cartwright and Santamarina, 2015).

### *5.2 Formation mechanism of pipes in the study area*

Hydraulic fracturing is the most frequently documented formation mechanism for fluid-escape pipes along continental margins (Holford et al., 2017; Jamtveit et al., 2004). The process involves the development of overpressure in an underlying root zone, which induces fracturing of the overburden. Subsequently, fractures propagate upwards in a direction normal to the minimum stress and widen with increasing height (Cartwright and Santamarina, 2015b). Accordingly, Cartwright et al., (2021) conducted an experimental study to investigate the pressure conditions required for the formation of fluid escape pipes in sedimentary basins. Their results showed that pipes form when the overpressure is more than 30 MPa, with pressure recharge of up to 2 MPa occurring after each pipe-forming event. This led to sawtooth pressure-time evolution. The experimental model used by the authors consists of 21 fluid escape pipes that transected 3 km of claystone and evaporite sealing units over an interval of 50–100 k.y. to finally reach the seabed. Localized collapse by volume loss is a common formation mechanism in carbonate or limestone dominated sequences (Bertoni and Cartwright, 2005). Other mechanisms, such as erosive fluidization, capillary invasion, and syn-sedimentary flow localization, have only been identified through experimental works (Liu and Flemings, 2006; Nichols et al., 1994).

Root zones found in proximity to sediment drifts or contourite mounds in the study area suggest that subsurface strata beneath U4 are associated with overpressure at depth. Contourite mounds serve as pressure foci and can form gas columns due to structural closure (Cartwright and Santamarina 2015). The sediment in the drifts may include underconsolidated, fine-grained, low-permeability, and high-porosity siliceous ooze layers, along with excess pore pressure (Volpi et al., 2003). The likely triggers for the overpressure observed in the study area may include overburden pressure, rapid sedimentation, and tectonic stresses active during the Neogene-Quaternary. Hydrofracturing would lead to the formation of a pipe structure, which can transport overpressure to shallower subsurface layers. If the overpressure reservoir is large compared to the fracture volume in the pipe, pore water, free gas and dissolved gas can migrate upwards, thus sustaining the overpressure (Elger et al., 2018).

### *5.3 Impact of lithology during initiation and modulation of pipes*

Highly layered, clay-dominated marine sedimentary successions, typically of Neogene age have accounted for most pipes known from seismic reflection data in passive continental margins (Cartwright and Santamarina 2015). There might be several other pipes buried in deeper stratigraphic intervals. However, their imaging has been hampered by high frequency attenuation in older and deeper sedimentary formations (Yilmaz, 2001). Pipes are mainly known from clastic lithologies and only described in carbonate settings where they were associated with dissolution structures e.g., Bertoni and Cartwright, 2005. The interaction of fluid-escape pipes with geobodies or large and thick sediment piles such as mass-transport complexes and contourites is well documented in the literature. Mass-transport complexes (MTCs) can play an important role in the formation of fluid escape pipes by eroding former strata and creating effusion of fluid in potential reservoirs (Cardona et al., 2020). Pipes can also occur in close association with the basal slide zone of seismic-scale MTCs or formed due to rapid loading of a sedimentary succession by the emplacement of several meter thick MTCs. The latter relationship has been seen as a process advancing recurrent slope instability on some continental margins (see Browne et al., 2020). Similarly, contourites are known to develop in basin with history of protracted fluid seepage where topographic roughness created by pockmarks can influence the formation of mounded contourites (Waghorn et al., 2018). This creates a cause-effect relationship between fluid expulsion and the deposition of contouritic drifts.

The 3D lithological models show how lithology influences the preferential positioning of pipes in the study area. Here, pipes are often buried or truncated amid heterogeneous strata made up of mud and sands (Figures 12 and 13), and they cross thick units of Neogene strata (up to 800 m) in this area. Figures 13c and 13d, for example, show that most pipes are in regions with low to intermediate sand potential, indicating that pipes have a high affinity for mud-rich sediments. The inverted data allowed

for the resolution of the heterogeneity of these units at the scale of seismic observation to mud and sand only. Yet, the well data show that other types of silt, like muddy sand and shell hash, can also be present in the sediment (Figure 11). Despite this, the root zones largely crossed layers of mud and sand-rich successions while the higher units are essentially mud-rich. This interpretation and 3D model of paleoshelves that are distinguished by clastic lithologies are also supported by the interactions of the pipes with the sediment drifts.

## 6. Conclusions

This study investigates the influence of basin and depositional setting on the initiation and growth of fluid-escape pipes in the Canterbury Basin, utilizing three-dimensional seismic reflection and borehole data to characterize lithology and decipher the timing and origin of the pipes. Our results indicate that pipes are vertical to sub-vertical and upward widening structures on seismic reflection data, with a distinct architecture consisting of a top, main conduit/stem, and a root zone, and seismic facies characterized by low amplitude, transparent, distorted, or down-warped reflections. These pipes formed post-Tarantian (0.113 Ma) and originated from multiple, overpressured stratigraphic strata and structures within the Neogene-Quaternary interval. They play a vital role in enabling cross-stratal fluid movement from the subsurface to near and onto the seafloor. The initiation and modulation of pipes are influenced by key basin and depositional structures, including lithology and geomorphologic structures such as contourite mounds. In our study area, pipes are rooted at the tops of contourite mounds or on the flanks of sediment drifts, crossing thick, heterogenous clastic lithologies dominated by mud. The development of overpressure in the underlying root zones likely induces hydraulic fracturing and growth of the pipes. We also found bright spots indicative of fluid accumulation in the subsurface, associated with pipe tops, suggesting the interaction of both vertical and lateral fluid conduits or cells in the study area. These findings highlight the importance of lithology and geomorphologic structure in the preferential siting of pipes in the Canterbury Basin and have implications for understanding the formation of fluid-escape pipes along continental margins.

## References

- Alves, T.M., Omosanya, K., Gowling, P., 2015. Volume rendering of enigmatic high-amplitude anomalies in southeast Brazil: A workflow to distinguish lithologic features from fluid accumulations. *Interpretation* 3, A1–A14.
- Anderson, A.L., Hampton, L.D., 1980. Acoustics of gas-bearing sediments I. Background. *The Journal of the Acoustical Society of America* 67, 1865–1889.
- Andresen, K.J., 2012. Fluid flow features in hydrocarbon plumbing systems: What do they tell us about the basin evolution? *Marine Geology* 332–334, 89–108. <https://doi.org/10.1016/j.margeo.2012.07.006>
- Berndt, C., 2005. Focused fluid flow in passive continental margins. *Phil. Trans. R. Soc. A* 363, 2855–2871. <https://doi.org/10.1098/rsta.2005.1666>
- Berndt, C., Büinz, S., Mienert, J., 2003. Polygonal fault systems on the mid-Norwegian margin: a long-term source for fluid flow. *SP 216*, 283–290. <https://doi.org/10.1144/GSL.SP.2003.216.01.18>
- Berndt, C., Costa, S., Canals, M., Camerlenghi, A., de Mol, B., Saunders, M., 2012. Repeated slope failure linked to fluid migration: The Ana submarine landslide complex, Eivissa Channel, Western Mediterranean Sea. *Earth and Planetary Science Letters* 319–320, 65–74. <https://doi.org/10.1016/j.epsl.2011.11.045>
- Bertoni, C., Cartwright, J.A., 2005. 3D seismic analysis of circular evaporite dissolution structures, Eastern Mediterranean. *Journal of the Geological Society* 162, 909–926. <https://doi.org/10.1144/0016-764904-126>
- Böttner, C., Callow, B.J., Schramm, B., Gross, F., Geersen, J., Schmidt, M., Vasilev, A., Petsinski, P., Berndt, C., 2021. Focused methane migration formed pipe structures in permeable sandstones:

Insights from uncrewed aerial vehicle-based digital outcrop analysis in Varna, Bulgaria. *Sedimentology* 68, 2765–2782. <https://doi.org/10.1111/sed.12871>

- Bradshaw, J.D., 1989. Cretaceous geotectonic patterns in the New Zealand Region. *Tectonics* 8, 803–820. <https://doi.org/10.1029/TC008i004p00803>
- Browne, G.H., Bull, S., Arnot, M.J., Boyes, A.F., King, P.R., Helle, K., 2020. The role of mass transport deposits contributing to fluid escape: Neogene outcrop and seismic examples from north Taranaki, New Zealand. *Geo-Mar Lett* 40, 789–807. <https://doi.org/10.1007/s00367-020-00641-z>
- Browne, G.H., Field, B.D., 1988. A review of Cretaceous–Cenozoic sedimentation and tectonics, east coast, South Island, New Zealand. *Mem.—Can. Soc. Pet. Geol* 15, 37–48.
- Browne, G.H., Naish, T.R., 2003. Facies development and sequence architecture of a late Quaternary fluvial-marine transition, Canterbury Plains and shelf, New Zealand: implications for forced regressive deposits. *Sediment. Geol* 158, 57–86. [https://doi.org/doi:10.1016/S0037-0738\(02\)00258-0](https://doi.org/doi:10.1016/S0037-0738(02)00258-0)
- Cardona, S., Wood, L., Moscardelli, L., Dunlap, D., 2020. Cannibalization and sealing of deepwater reservoirs by mass-transport complexes — The Jubilee field, Gulf of Mexico. *Interpretation* 8, SV17–SV30. <https://doi.org/10.1190/INT-2019-0274.1>
- Carter, R.M., 1988. Post-breakup stratigraphy of the Kaikoura Synthem (Cretaceous–Cenozoic), continental margin, southeastern New Zealand. *N. Z. J. Geol. Geophys* 31, 405–429.
- Carter, R.M., Norris, R.J., 1976. Cainozoic history of southern New Zealand: an accord between geological observations and plate-tectonic predictions. *Earth Planet. Sci. Lett* 31, 85–94. [https://doi.org/doi:10.1016/0012-821X\(76\)90099-6](https://doi.org/doi:10.1016/0012-821X(76)90099-6)
- Cartwright, J., Huuse, M., Aplin, A., 2007. Seal bypass systems. *Bulletin* 91, 1141–1166. <https://doi.org/10.1306/04090705181>
- Cartwright, J., Kirkham, C., Foschi, M., Hodgson, N., Rodriguez, K., James, D., 2021. Quantitative reconstruction of pore-pressure history in sedimentary basins using fluid escape pipes. *Geology* 49, 576–580. <https://doi.org/10.1130/G48406.1>
- Cartwright, J., Santamarina, C., 2015. Seismic characteristics of fluid escape pipes in sedimentary basins: Implications for pipe genesis. *Marine and Petroleum Geology* 65, 126–140. <https://doi.org/10.1016/j.marpetgeo.2015.03.023>
- Chen, D., Zhang, G., Wang, X., Wang, Z., Chen, S., Dong, D., 2021a. Seismic features and origin of fluid escape pipes offshore Hainan Island on the northern slope of South China Sea. *Marine and Petroleum Geology* 133, 105276.
- Chen, D., Zhang, G., Wang, X., Wang, Z., Chen, S., Dong, D., 2021b. Seismic features and origin of fluid escape pipes offshore Hainan Island on the northern slope of South China Sea. *Marine and Petroleum Geology* 133, 105276. <https://doi.org/10.1016/j.marpetgeo.2021.105276>
- Elger, J., Berndt, C., Rüpke, L., Krastel, S., Gross, F., Geissler, W.H., 2018a. Submarine slope failures due to pipe structure formation. *Nat Commun* 9, 715. <https://doi.org/10.1038/s41467-018-03176-1>
- Elger, J., Berndt, C., Rüpke, L., Krastel, S., Gross, F., Geissler, W.H., 2018b. Submarine slope failures due to pipe structure formation. *Nat Commun* 9, 715. <https://doi.org/10.1038/s41467-018-03176-1>
- Elliot, D.H., Grimes, C.G., 2011. Triassic and Jurassic strata at Coombs Hills, south Victoria Land: stratigraphy, petrology and cross-cutting breccia pipes. *Antarctic science* 23, 268–280. <https://doi.org/10.1017/S0954102010000994>

- Field, B.D., Browne, G.H., 1989. Cretaceous and Cenozoic Sedimentary Basins and Geological Evolution of Canterbury Region, South Island, New Zealand. *N. Z. Geol. Surv., Basin Stud* 2.
- Fulthorpe, C.S., Carter, R.M., 1991. Continental-shelf progradation by sediment-drift accretion. *Geol. Soc. Am. Bull* 103, 300–309. [https://doi.org/doi:10.1130/0016-7606\(1991\)103<0300:CSPBSD>2.3.CO;2](https://doi.org/doi:10.1130/0016-7606(1991)103<0300:CSPBSD>2.3.CO;2)
- Fulthorpe, C.S., Carter, R.M., Miller, K.G., Wilson, J., 1996. Marshall paraconformity: a mid-Oligocene record of inception of the Antarctic Circumpolar Current and coeval glacio-eustatic lowstand? *Mar. Pet. Geol* 13, 61–77. [https://doi.org/doi:10.1016/0264-8172\(95\)00033-X](https://doi.org/doi:10.1016/0264-8172(95)00033-X)
- Fulthorpe, C.S., Hoyanagi, K., Blum, P., Expedition 317 Scientists (Eds.), 2011. Proceedings of the IODP, 317, Proceedings of the IODP. Integrated Ocean Drilling Program. <https://doi.org/10.2204/iodp.proc.317.2011>
- Grove, C., 2013. Submarine hydrothermal vent complexes in the Paleocene of the Faroe-Shetland Basin: Insights from three-dimensional seismic and petrographical data. *Geology* 41, 71–74. <https://doi.org/10.1130/G33559.1>
- Hawkes, P.W., Mound, D.G., 1984. Clipper-1 geological completion report. *N. Z. Geol. Surv. Open-File Rep.*
- Holford, S.P., Schofield, N., Reynolds, P., 2017. Subsurface fluid flow focused by buried volcanoes in sedimentary basins: Evidence from 3D seismic data, Bass Basin, offshore southeastern Australia. *Interpretation* 5, SK39–SK50. <https://doi.org/10.1190/INT-2016-0205.1>
- Hovland, M., Judd, A.G., 1988. Seabed Pockmarks and Seepages. Impact on Geology, Biology and the Marine Environment. Graham and Trotman Ltd, London.
- Hurst, A., Scott, A., Vigorito, M., 2011. Physical characteristics of sand injectites. *Earth-Science Reviews* 106, 215–246. <https://doi.org/10.1016/j.earscirev.2011.02.004>
- Hustoft, S., Mienert, J., Bünz, S., Nouzé, H., 2007. High-resolution 3D-seismic data indicate focussed fluid migration pathways above polygonal fault systems of the mid-Norwegian margin. *Marine Geology* 245, 89–106. <https://doi.org/10.1016/j.margeo.2007.07.004>
- Huuse, M., Shoulders, S.J., Netoff, D.I., Cartwright, J., 2005. Giant sandstone pipes record basin-scale liquefaction of buried dune sands in the Middle Jurassic of SE Utah. *Terra Nova* 17, 80–85. <https://doi.org/10.1111/j.1365-3121.2004.00587.x>
- Huuse, M., Van Rensbergen, P., Jackson, C.A.-L., Flemings, P.B., Davies, R.J., Dixon, R.J., 2010. Subsurface sediment remobilization and fluid flow in sedimentary basins: preface. *Basin Research* 22, 341–341. <https://doi.org/10.1111/j.1365-2117.2010.00487.x>
- Ismail, A., Ewida, H.F., Al-Ibiary, M.G., Gammaldi, S., Zollo, A., 2020. Identification of gas zones and chimneys using seismic attributes analysis at the Scarab field, offshore, Nile Delta, Egypt. *Petroleum Research* 5, 59–69. <https://doi.org/10.1016/j.ptlrs.2019.09.002>
- Jamtveit, B., Svensen, H., Podladchikov, Y.Y., Planke, S., 2004. Hydrothermal vent complexes associated with sill intrusions in sedimentary basins. *Physical Geology of High-Level Magmatic Systems*. Geological Society, London, Special Publications 234, 233–241.
- Johannessen, E.P., Steel, R.J., 2005. Shelf-margin clinofolds and prediction of deepwater sands. *Basin Research* 17, 521–550. <https://doi.org/10.1111/j.1365-2117.2005.00278.x>
- Judd, A., Hovland, M., 2007. Seabed Fluid Flow: The Impact on Geology, Biology and the Marine Environment. Cambridge University Press.
- Kamp, P.J.J., 1986. The mid-Cenozoic Challenger Rift System of western New Zealand and its implications for the age of Alpine fault inception. *GSA Bulletin* 97, 255–281. [https://doi.org/10.1130/0016-7606\(1986\)97<255:TMCRSO>2.0.CO;2](https://doi.org/10.1130/0016-7606(1986)97<255:TMCRSO>2.0.CO;2)

- King, P.R., 2000. Tectonic reconstructions of New Zealand: 40 Ma to the present. *N. Z. J. Geol. Geophys* 43, 611–638.
- Kirkham, C., Cartwright, J., Bertoni, C., Rodriguez, K., Hodgson, N., 2019. An insight Into the 3D Kinematics of a Thick Salt Sheet Using Fluids Escape Pipes as Natural Markers for Deformation, in: 81st EAGE Conference and Exhibition 2019. Presented at the 81st EAGE Conference and Exhibition 2019, European Association of Geoscientists & Engineers, London, UK, pp. 1–5. <https://doi.org/10.3997/2214-4609.201900910>
- Leduc, A.M., Davies, R.J., Swarbrick, R.E., Imber, J., 2013. Fluid flow pipes triggered by lateral pressure transfer in the deepwater western Niger Delta. *Marine and Petroleum Geology* 43, 423–433. <https://doi.org/10.1016/j.marpetgeo.2012.12.005>
- Liu, X., Flemings, P.B., 2006. Passing gas through the hydrate stability zone at southern Hydrate Ridge, offshore Oregon. *Earth and Planetary Science Letters* 241, 211–226. <https://doi.org/10.1016/j.epsl.2005.10.026>
- Løseth, H., Gading, M., Wensaas, L., 2009. Hydrocarbon leakage interpreted on seismic data. *Marine and Petroleum Geology* 26, 1304–1319. <https://doi.org/10.1016/j.marpetgeo.2008.09.008>
- Løseth, H., Wensaas, L., Arntsen, B., Hanken, N.-M., Basire, C., Graue, K., 2011. 1000 m long gas blow-out pipes. *Marine and Petroleum Geology* 28, 1047–1060. <https://doi.org/10.1016/j.marpetgeo.2010.10.001>
- Lu, H., Fulthorpe, C.S., 2004. Controls on sequence stratigraphy of a middle Miocene–Holocene, current-swept, passive margin: offshore Canterbury Basin, New Zealand. *Geol. Soc. Am. Bull* 116, 1345–1366. <https://doi.org/doi:10.1130/B2525401.1>
- Lu, H., Fulthorpe, C.S., Mann, P., 2003. Three-dimensional architecture of shelf-building sediment drifts in the offshore Canterbury Basin, New Zealand. *Mar. Geol* 193, 19–47. [https://doi.org/doi:10.1016/S0025-3227\(02\)00612-6](https://doi.org/doi:10.1016/S0025-3227(02)00612-6)
- Maestrelli, D., Iacopini, D., Jihad, A.A., Bond, C.E., Bonini, M., 2017. Seismic and structural characterization of fluid escape pipes using 3D and partial stack seismic from the Loyal Field (Scotland, UK): A multiphase and repeated intrusive mechanism. *Marine and Petroleum Geology* 88, 489–510. <https://doi.org/10.1016/j.marpetgeo.2017.08.016>
- Manton, B., Müller, P., Mazzini, A., Zastrozhnov, D., Jerram, D.A., Millett, J.M., Schmid, D.W., Berndt, C., Myklebust, R., Planke, S., 2022. Characterizing ancient and modern hydrothermal venting systems. *Marine Geology* 447, 106781. <https://doi.org/10.1016/j.margeo.2022.106781>
- Mazzini, A., Lupi, M., Sciarra, A., Hamed, M., Schmidt, S.T., Suessenberger, A., 2019. Concentric Structures and Hydrothermal Venting in the Western Desert, Egypt. *Front. Earth Sci.* 7, 266. <https://doi.org/10.3389/feart.2019.00266>
- McHugh, C.M., Fulthorpe, C.S., Hoyanagi, K., Blum, P., Mountain, G.S., Miller, K.G., 2018. The sedimentary imprint of Pleistocene glacio-eustasy: Implications for global correlations of seismic sequences. *Geosphere* 14, 265–285. <https://doi.org/10.1130/GES01569.1>
- Mohammedyasin, S., Lippard, S.J., Omosanya, K.O., Johansen, S.E., Harishidayat, D., 2016. Deep-seated faults and hydrocarbon leakage in the Snøhvit Gas Field, Hammerfest Basin, Southwestern Barents Sea.
- Molnar, P., Atwater, T., Mammerickx, J., Smith, S., 1975. Magnetic anomalies, bathymetry and the tectonic evolution of the South Pacific since the Late Cretaceous. *Geophys. J. R. Astron. Soc* 40, 383–420.
- Moss, J.L., Cartwright, J., 2010. 3D seismic expression of km-scale fluid escape pipes from offshore Namibia. *Basin Research* 22, 481–501.

- Neumann, E.-R., Svensen, H.H., Polozov, A.G., Hammer, Ø., 2017. Formation of Si-Al-Mg-Ca-rich zoned magnetite in an end-Permian phreatomagmatic pipe in the Tunguska Basin, East Siberia. *Miner Deposita* 52, 1205–1222. <https://doi.org/10.1007/s00126-017-0717-9>
- Nichols, R.J., Sparks, R.S.J., Wilson, C.J.N., 1994. Experimental studies of the fluidization of layered sediments and the formation of fluid escape structures. *Sedimentology* 41, 233–253. <https://doi.org/10.1111/j.1365-3091.1994.tb01403.x>
- Norris, R.J., Carter, R.M., Turnbull, I.M., 1978. Cainozoic sedimentation in basins adjacent to a major continental transform boundary in southern New Zealand. *J. Geol. Soc. (London, U. K)* 135, 191–205. <https://doi.org/doi:10.1144/gsjgs.135.2.0191>
- Norris, R.J., Cooper, A.F., 2001. Late Quaternary slip rates and slip partitioning on the Alpine Fault, New Zealand. *Journal of Structural Geology* 23, 507–520. [https://doi.org/10.1016/S0191-8141\(00\)00122-X](https://doi.org/10.1016/S0191-8141(00)00122-X)
- Omosanya, K., Ajibola, L.M., Muhammad, I.H., Makovsky, Y., 2021. Massive seafloor mounds depict potential for seafloor mineral deposits in the Great South Basin (GSB) offshore New Zealand. *Sci Rep* 11, 9185. <https://doi.org/10.1038/s41598-021-88620-x>
- Omosanya, K.O., Harishidayat, D., Marheni, L., Johansen, S.E., Felix, M., Abrahamson, P., 2016. Recurrent mass-wasting in the Sørvestsnaget Basin Southwestern Barents Sea: A test of multiple hypotheses. *Marine Geology* 376, 175–193. <https://doi.org/10.1016/j.margeo.2016.03.003>
- Omosanya, K.O., Maia, A.R., Eruteya, O.E., 2020. Seismic, morphologic and scale variabilities of subsurface pipes and vent complexes in a magma-rich margin. *Bull Volcanol* 82, 40. <https://doi.org/10.1007/s00445-020-01379-3>
- Oppo, D., Evans, S., Iacopini, D., Kabir, S.M., Maselli, V., Jackson, C.A.-L., 2021. Leaky salt: Pipe trails record the history of cross-evaporite fluid escape in the northern Levant Basin, Eastern Mediterranean. *Basin Research* 33, 1798–1819.
- Paganoni, M., Cartwright, J.A., Foschi, M., Shipp, C.R., Van Rensbergen, P., 2018. Relationship between fluid-escape pipes and hydrate distribution in offshore Sabah (NW Borneo). *Marine Geology* 395, 82–103.
- Planke, S., Berndt, C., Alvarez Zarikian, C.A., 2022. Expedition 396 Preliminary Report: Mid-Norwegian Margin Magmatism and Paleoclimate Implications, International Ocean Discovery Program Preliminary Report. *International Ocean Discovery Program*. <https://doi.org/10.14379/iodp.pr.396.2022>
- Ruge, S.M., Scarselli, N., Bilal, A., 2021. 3D seismic classification of fluid escape pipes in the western Exmouth Plateau, Northwest Shelf of Australia. *JGS* 178, jgs2020-096. <https://doi.org/10.1144/jgs2020-096>
- Safronova, P.A., Henriksen, S., Andreassen, K., Laberg, J.S., Vorren, T.O., 2014. Evolution of shelf-margin clinoforms and deep-water fans during the middle Eocene in the Sørvestsnaget Basin, southwest Barents Sea. *Bulletin* 98, 515–544. <https://doi.org/10.1306/08221312208>
- Schiøler, P., Raine, J.I., Crundwell, M., Griffin, A.G., Hollis, C.J., Kulhanek, D.K., Morgan, H.E.G., Roncaglia, L., Strong, C.P., Uruski, C., 2011. Revised biostratigraphy and well correlation, Canterbury Basin, New Zealand. (Consultancy Report No. GNS Science). New Zealand.
- Schroot, B.M., Schüttenhelm, R.T.E., 2003. Shallow gas and gas seepage: expressions on seismic and other acoustic data from the Netherlands North Sea. *Journal of Geochemical Exploration* 78–79, 305–309. [https://doi.org/10.1016/S0375-6742\(03\)00112-2](https://doi.org/10.1016/S0375-6742(03)00112-2)
- Sheriff, R.E., Geldart, L.P., 1995. *Exploration Seismology*, Second Edition. ed. Cambridge University Press.

- Sutherland, R., Browne, G., 2003. Canterbury basin offers potential on South Island, New Zealand. *Oil and Gas Journal* 101, 45–49.
- Sutherland, R., Eberhart-Phillips, D., Harris, R.A., Stern, T., Beavan, J., Ellis, S., Henrys, S., Cox, S., Norris, R.J., Berryman, K.R., Townend, J., Bannister, S., Pettinga, J., Leitner, B., Wallace, L., Little, T.A., Cooper, A.F., Yetton, M., Stirling, M., 2007. Do great earthquakes occur on the Alpine Fault in central South Island, New Zealand?, in: Okaya, D., Stern, Tim, Davey, F. (Eds.), *Geophysical Monograph Series*. American Geophysical Union, Washington, D. C., pp. 235–251. <https://doi.org/10.1029/175GM12>
- Svensen, H., Jamtveit, B., Planke, S., Chevallier, L., 2006. Structure and evolution of hydrothermal vent complexes in the Karoo Basin, South Africa. *JGS* 163, 671–682. <https://doi.org/10.1144/1144-764905-037>
- Szabó, N.P., 2011. Shale volume estimation based on the factor analysis of well-logging data. *Acta Geophys.* 59, 935. <https://doi.org/10.2478/s11600-011-0034-0>
- Taner, M.T., 2001. Seismic attributes. *Canadian Society of Exploration Geophysicists Recorder* 26, 48–56.
- Tippett, J.M., Kamp, P.J.J., 1993. The role of faulting in rock uplift in the Southern Alps. *New Zealand. N. Z. J. Geol. Geophys* 36, 497–504.
- Vail, P.R., Mitchum, R.M., Thompson, S., 1977. Seismic Stratigraphy and Global Changes of Sea Level, Part 4 Global Cycles of Relative Changes of Sea Level, in: *Seismic Stratigraphy — Applications to Hydrocarbon Exploration*. American Association of Petroleum Geologists. <https://doi.org/10.1306/M26490C6>
- Van Rensbergen, P., Rabaute, A., Colpaert, A., Ghislain, T.St., Mathijs, M., Bruggeman, A., 2007. Fluid migration and fluid seepage in the Connemara Field, Porcupine Basin interpreted from industrial 3D seismic and well data combined with high-resolution site survey data. *Int J Earth Sci (Geol Rundsch)* 96, 185–197. <https://doi.org/10.1007/s00531-005-0021-2>
- Volpi, V., Camerlenghi, A., Hillenbrand, C.-D., Rebesco, M., Ivaldi, R., 2003. Effects of biogenic silica on sediment compaction and slope stability on the Pacific margin of the Antarctic Peninsula: Effects of biogenic silica. *Basin Research* 15, 339–363. <https://doi.org/10.1046/j.1365-2117.2003.00210.x>
- Waghorn, K.A., Pecher, I., Strachan, L.J., Crutchley, G., Bialas, J., Coffin, R., Davy, B., Koch, S., Kroeger, K.F., Papenberg, C., Sarkar, S., SO.226 Scientific Party, 2018. Paleo-fluid expulsion and contouritic drift formation on the Chatham Rise, New Zealand. *Basin Res* 30, 5–19. <https://doi.org/10.1111/bre.12237>
- Wilson, I.R., 1985. Galleon-1 geological completion report. *N. Z. Geol. Surv. Open-File Rep.*
- Wood, R.A., Stagpoole, V.M., 2007. Validation of tectonic reconstructions by crustal volume balance: New Zealand through the Cenozoic. *GSA Bulletin* 119, 933–943. <https://doi.org/10.1130/B26018.1>
- Wu, N., Jackson, C.A. -L., Johnson, H.D., Hodgson, D.M., Clare, M.A., Nugraha, H.D., Li, W., 2021. The formation and implications of giant blocks and fluid escape structures in submarine lateral spreads. *Basin Res* 33, 1711–1730. <https://doi.org/10.1111/bre.12532>
- Yilmaz, Ö., 2001. *Seismic data analysis., Investigations in Geophysics No. 10.* Society of Exploration Geophysicists.

**Acknowledgements**

The seismic data used here were made available by the New Zealand Government through New Zealand Petroleum and Minerals ([www.nzpam.govt.nz](http://www.nzpam.govt.nz)) as part of the 'exploration data pack'. IOPD is thanked for access to the EXP314 borehole data Schlumberger is gratefully acknowledged for the provision of Petrel® for seismic interpretation at the Department of Geoscience, University of Malta. Aaron's Micallef participation in this work is funded by the European Research Council (ERC) under the European Union's Horizon 2020 research and innovation program (grant agreement No 677898 (MARCAN)).

**Data Availability**

MCS reflection data collected during RV Maurice Ewing cruise EW00-01 are available from <https://www.marine-geo.org/tools/search/entry.php?id=EW0001>, whereas the ODP and IODP data are available at <https://www.iodp.org/resources/access-data-and-samples>. The seismic data are available from the

## Figures

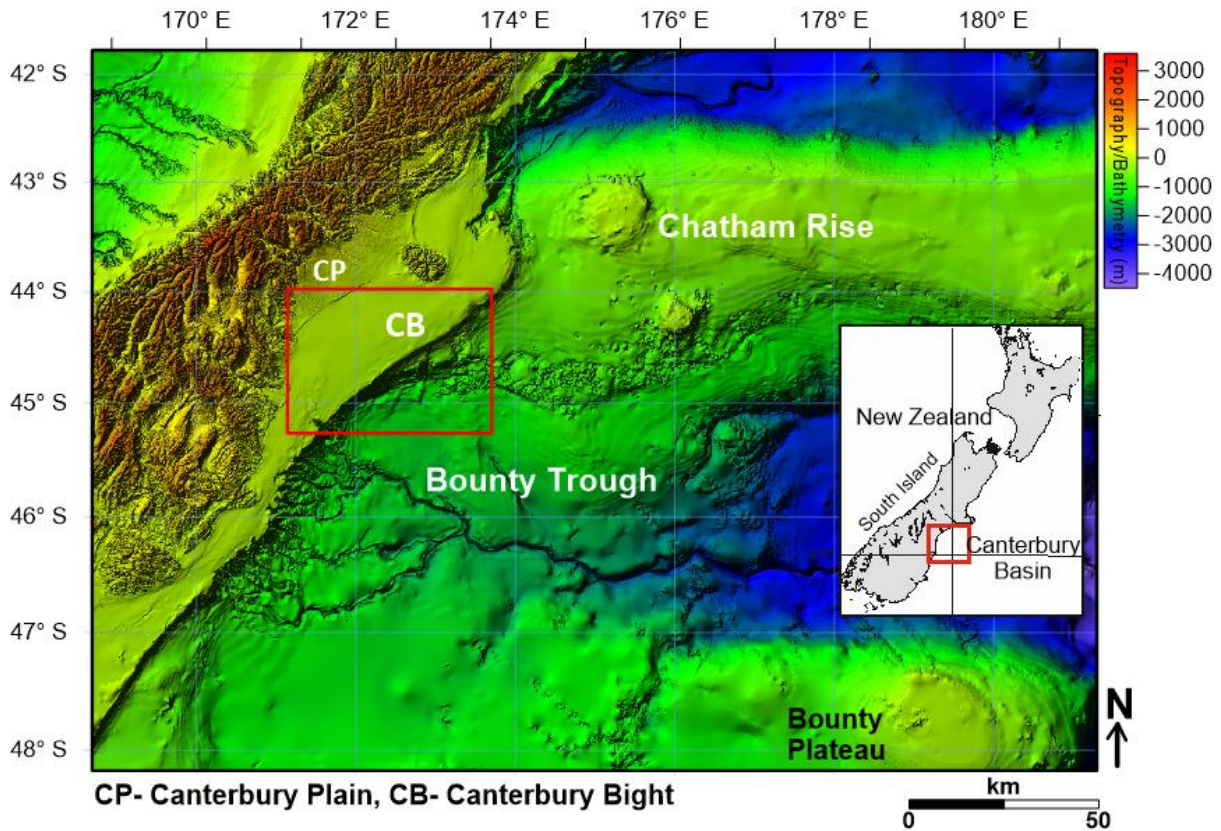


**Figure 1:** (a) Topographic and bathymetric map of the South Island of New Zealand. The bathymetry map was downloaded from <https://niwa.co.nz/our-science/oceans/bathymetry> and gridded in Surfer 8 ©. NB: The red rectangle shows the location of the Canterbury Basin and geophysical data used in this study. *Inset shows the location of the Canterbury Basin in the context of the Southern Island of New Zealand.*

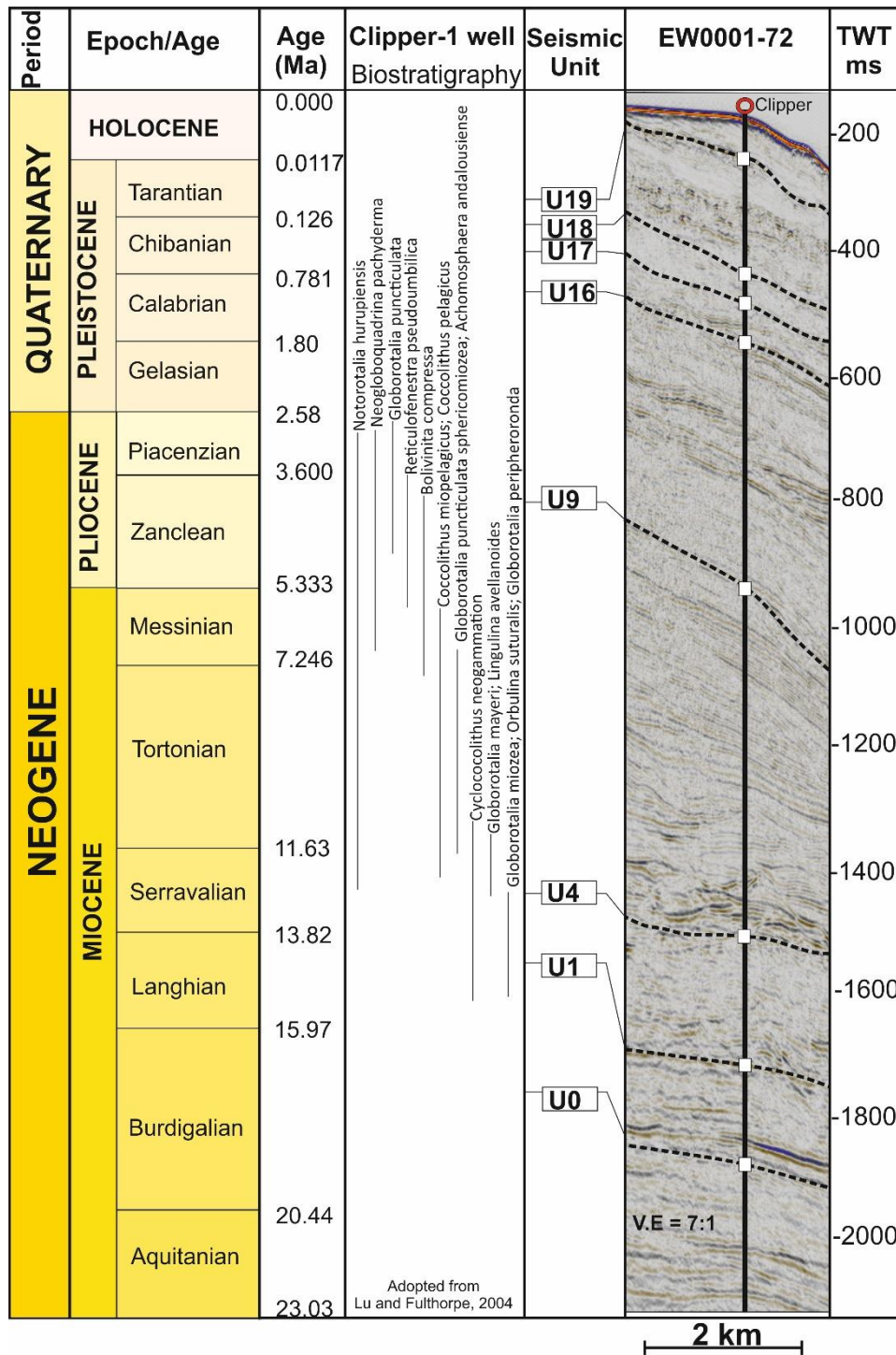


**Figure 2:** Lithostratigraphic column of the study area showing the ages of the interpreted horizons. The seismic-well tie was done on the Clipper-1 wellbore. The biostratigraphic information on nannofossils and foraminifera was adapted from the work of Lu and Fulthorpe, 2004.

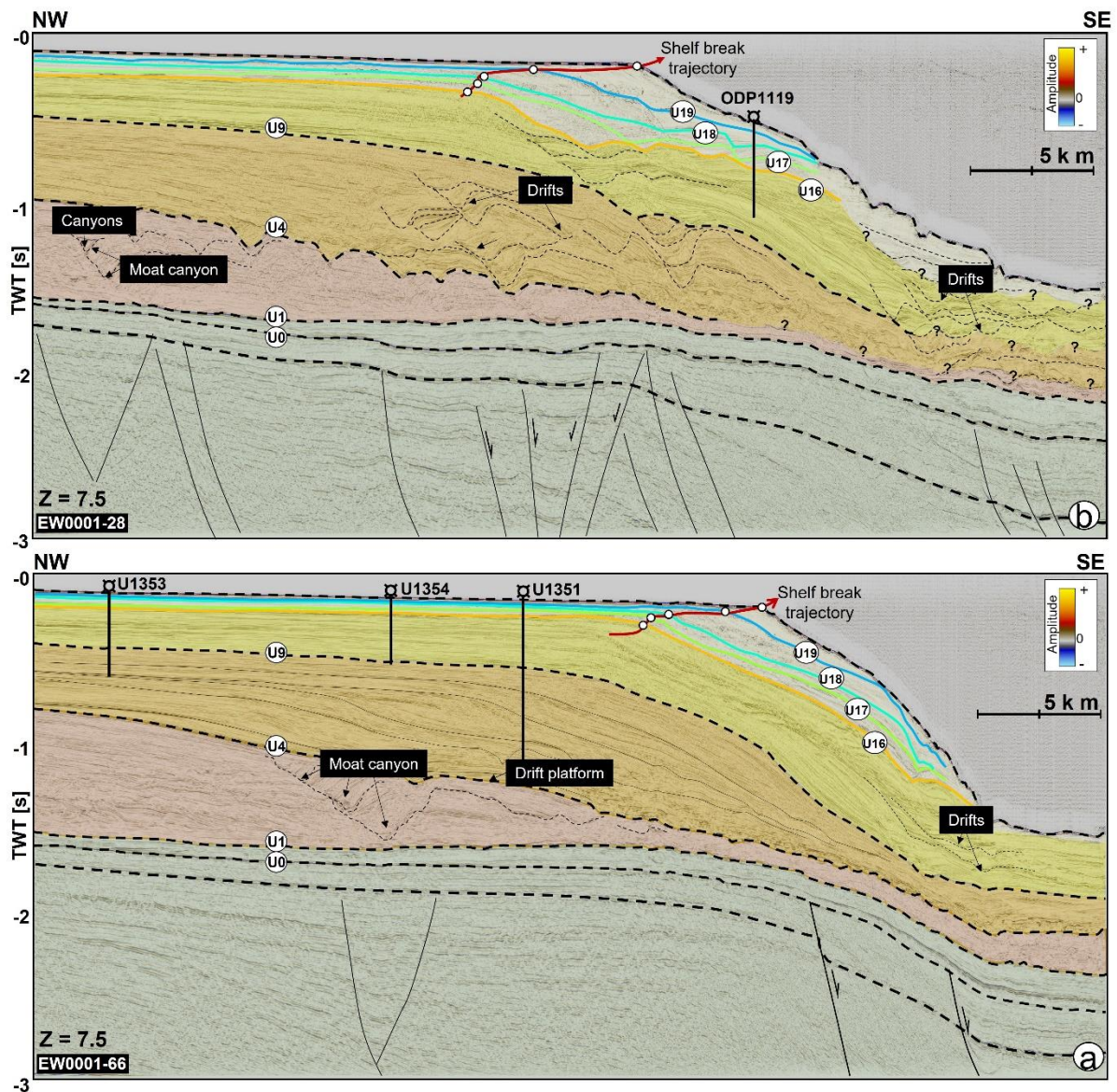


**Figure 3:** Interpreted seismic profiles (a) EW001-28 through the ODP 1119 wellbore and (b) EW001-66 through borehole sites U1353, U1354 and U1351 showing the overview geology of the Cenozoic interval in the Canterbury Basin. The Neogene interval are marked by different unconformities from U0-U19 and represent strata and lithologic facies deposited under the influence of bottom currents, glacial-interglacial cycles, and changes in eustatic sea-level. The intervals U0 to U4 were interpreted to find the root zones of the pipes. *Uninterpreted version of the seismic profiles are provided in the supplementary data.*

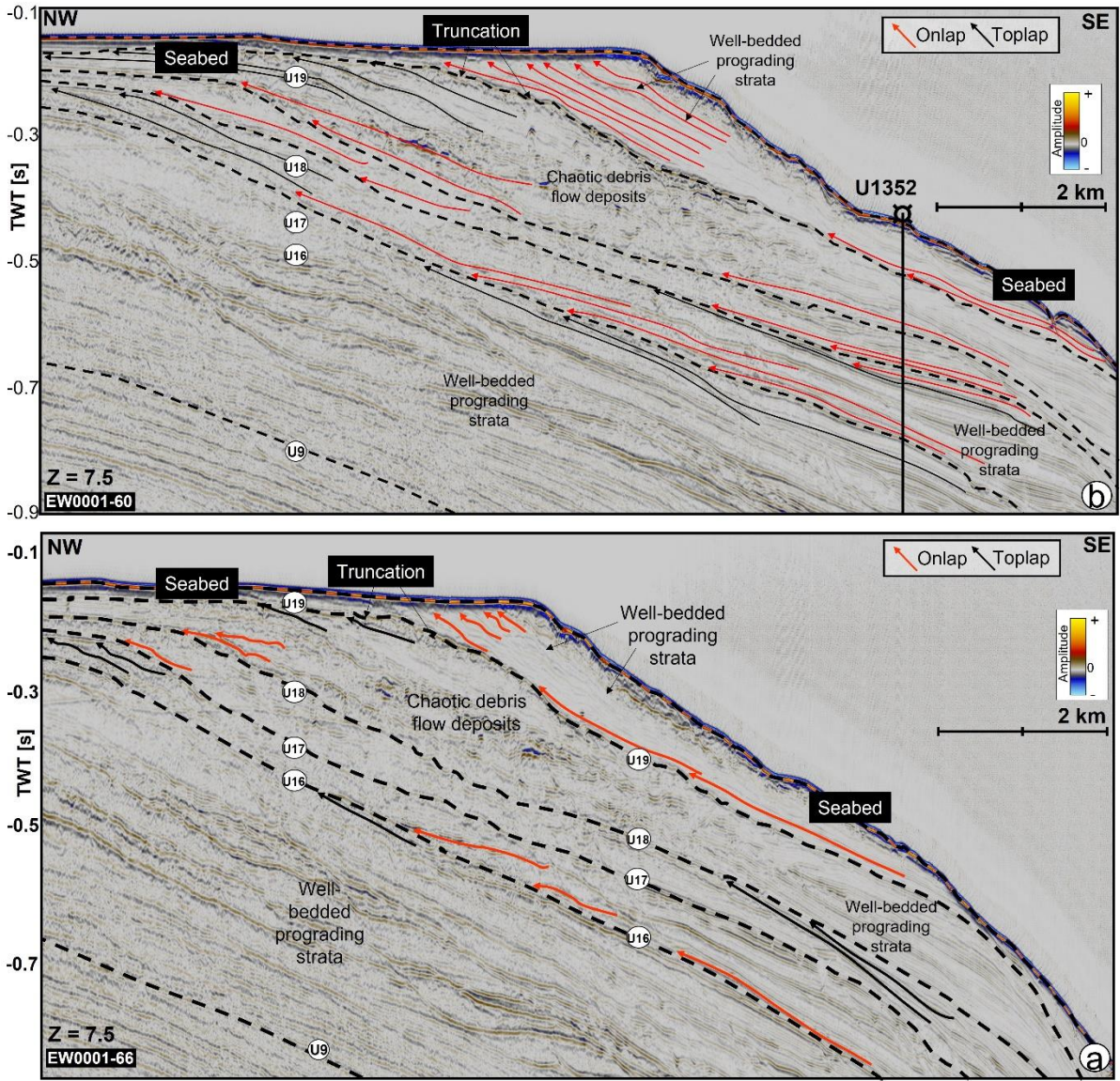


**Figure 4:** Interpreted seismic profiles (a) EW001-60 through site U1352 and (b) EW001-66 showing reflection termination and pattern at the shelf edge break of the study area. The intervals between U9 and U19 are characterized by different lithological and seismic facies such as well-bedded prograding strata and chaotic debris flow deposits reflecting changes in sedimentation pattern and infill during the latest Neogene times. *Uninterpreted version of the seismic profiles are provided in the supplementary data.*

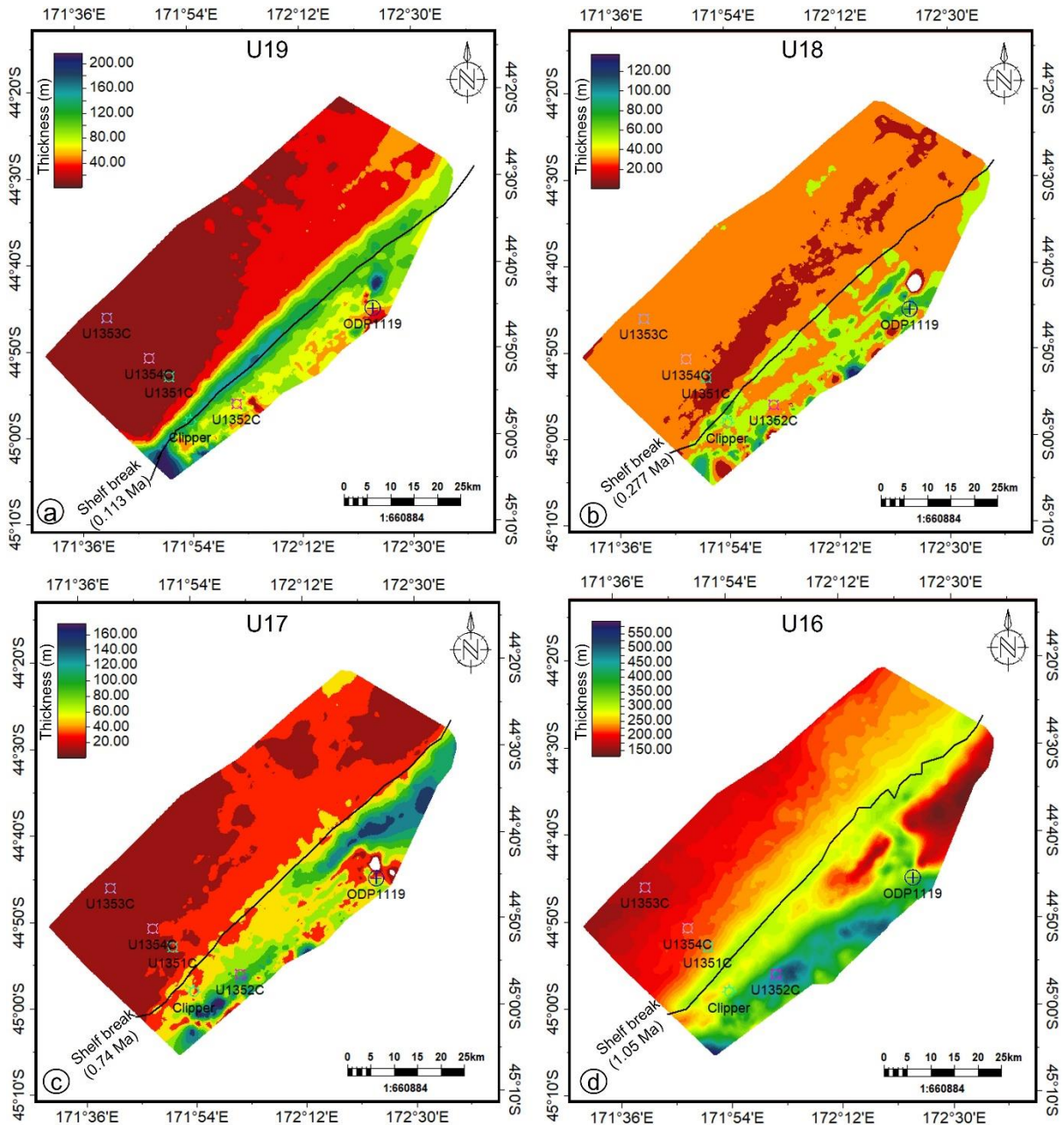


**Figure 5:** Stratigraphic thickness maps of (a) U19 (b) U18 (c) U17 and (d) U16 showing variation in sediment thickness of strata overlain by the main unconformities discussed in the text. Additionally, the variation in the position of the shelf break since 1.05 Ma is shown using the black strokes that run from NE-SW.

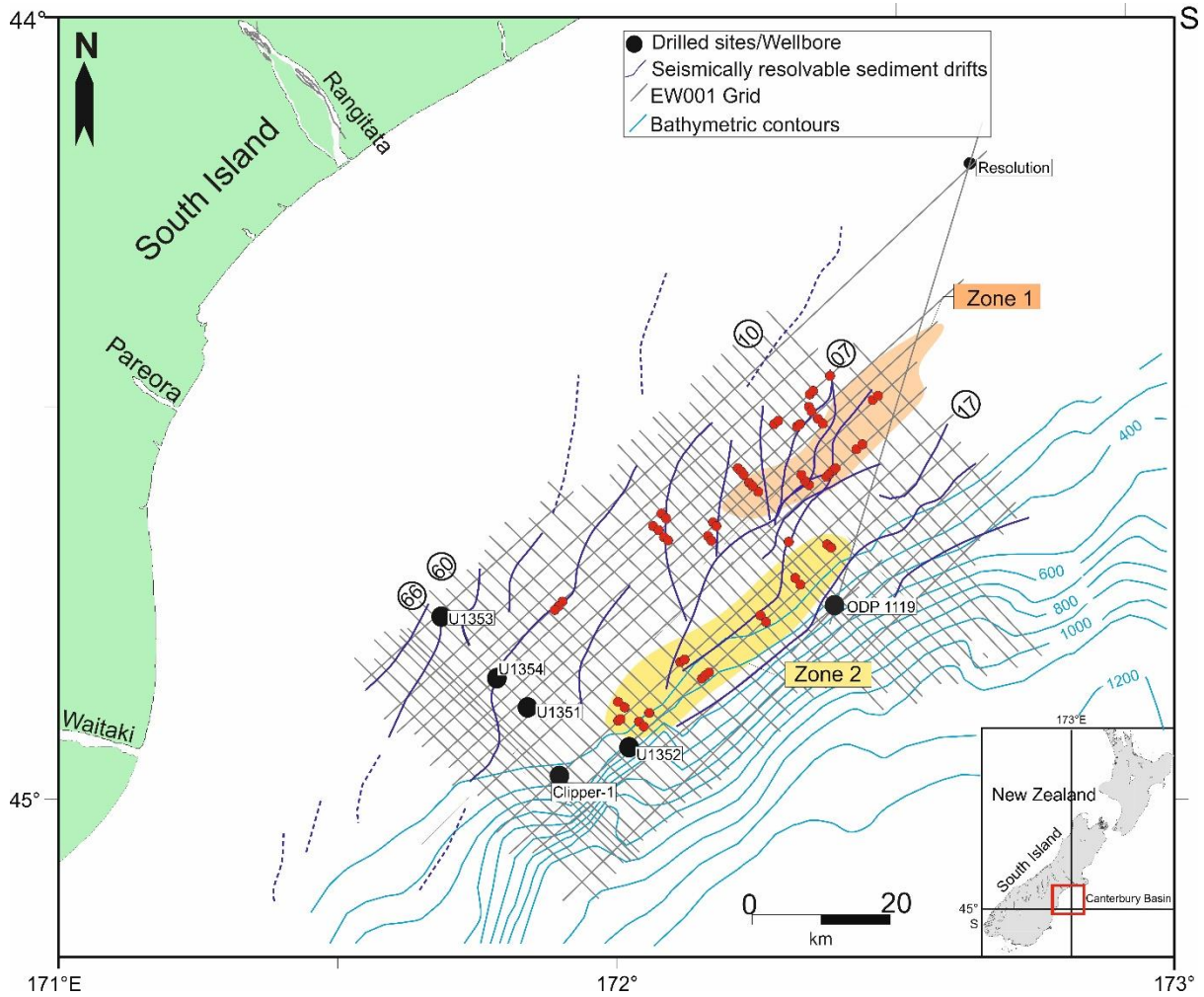


**Figure 6:** Facies map depicting the distribution of pipes interpreted in this work. Also shown is the connection between the pipes and subsurface geomorphologic structures such as contourite drifts in New Zealand's Canterbury Basin. Pipes in the subsurface are preferentially oriented along contourite drift trends, suggesting a cause-effect link between drift siting and pipe occurrence. In addition to the pipes, fluid related seismic anomalies in the study area can also include negative high amplitude anomalies found in Zone 1, flat and dispersed bright spots distributed around the paleo shelf-slope break in Zone 2. Note: The purple polylines represent seismically resolvable sediment drifts (Carter et al., 2004; Lu and Fulthorpe, 2004) while numbers in circle correspond to the location of the seismic lines described in the text. Inset shows the location of the Canterbury Basin in the context of the Southern Island of New Zealand.

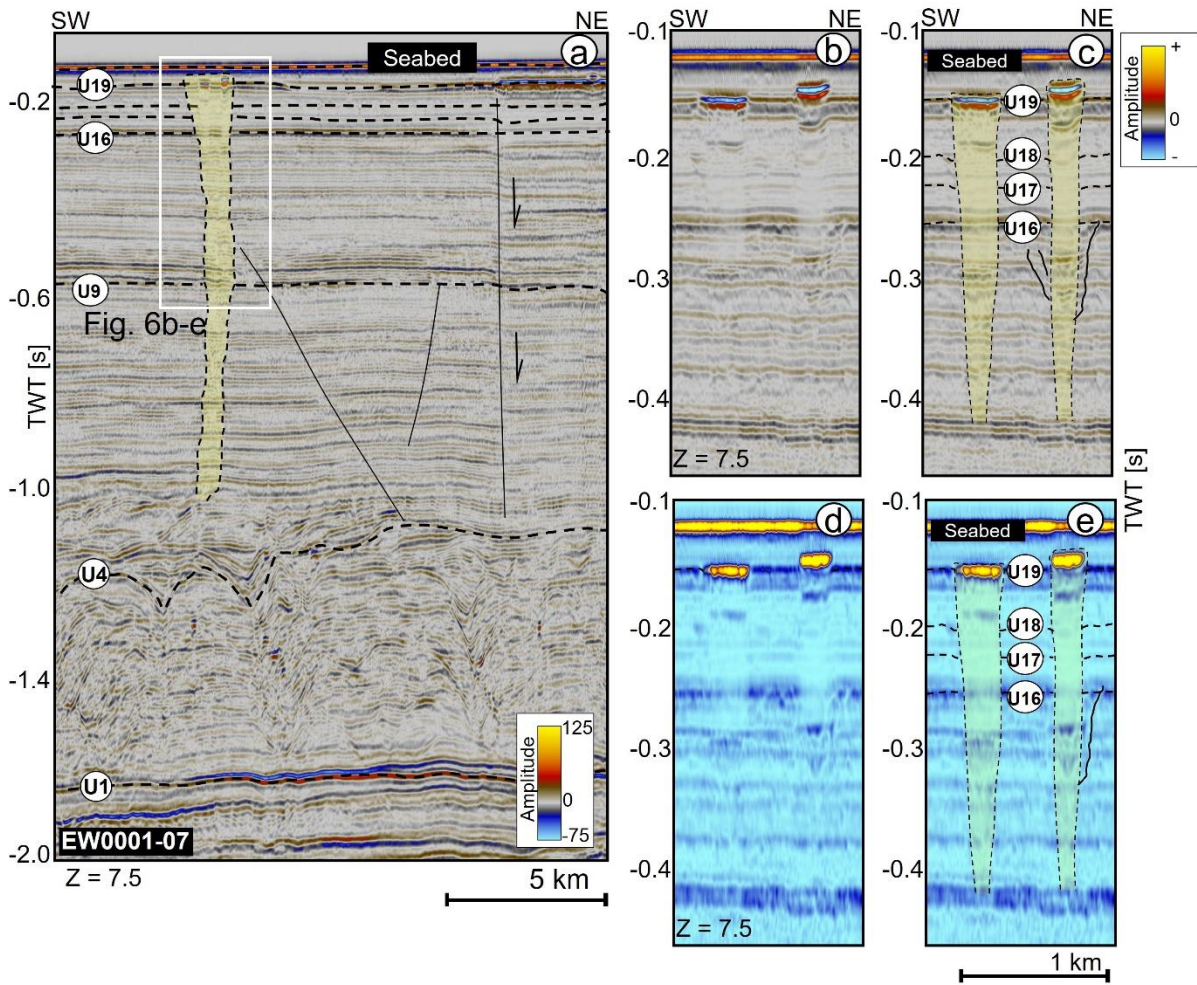


**Figure 7:** (a) Example of pipes rooted at the top of contourite drifts in the study area. Note: *Uninterpreted version of the seismic profile is provided in the supplementary data.* (b) and (c) Uninterpreted and interpreted seismic profiles showing seismic character of the two pipes in (a). The pipes have their zeniths above the U19 unconformity and their roots above U4. (d) and (e) Uninterpreted and interpreted envelope attribute profiles showing bright spot at the top of the pipes. These bright spots are positive high amplitude anomalies with the same polarity as the seabed reflection.

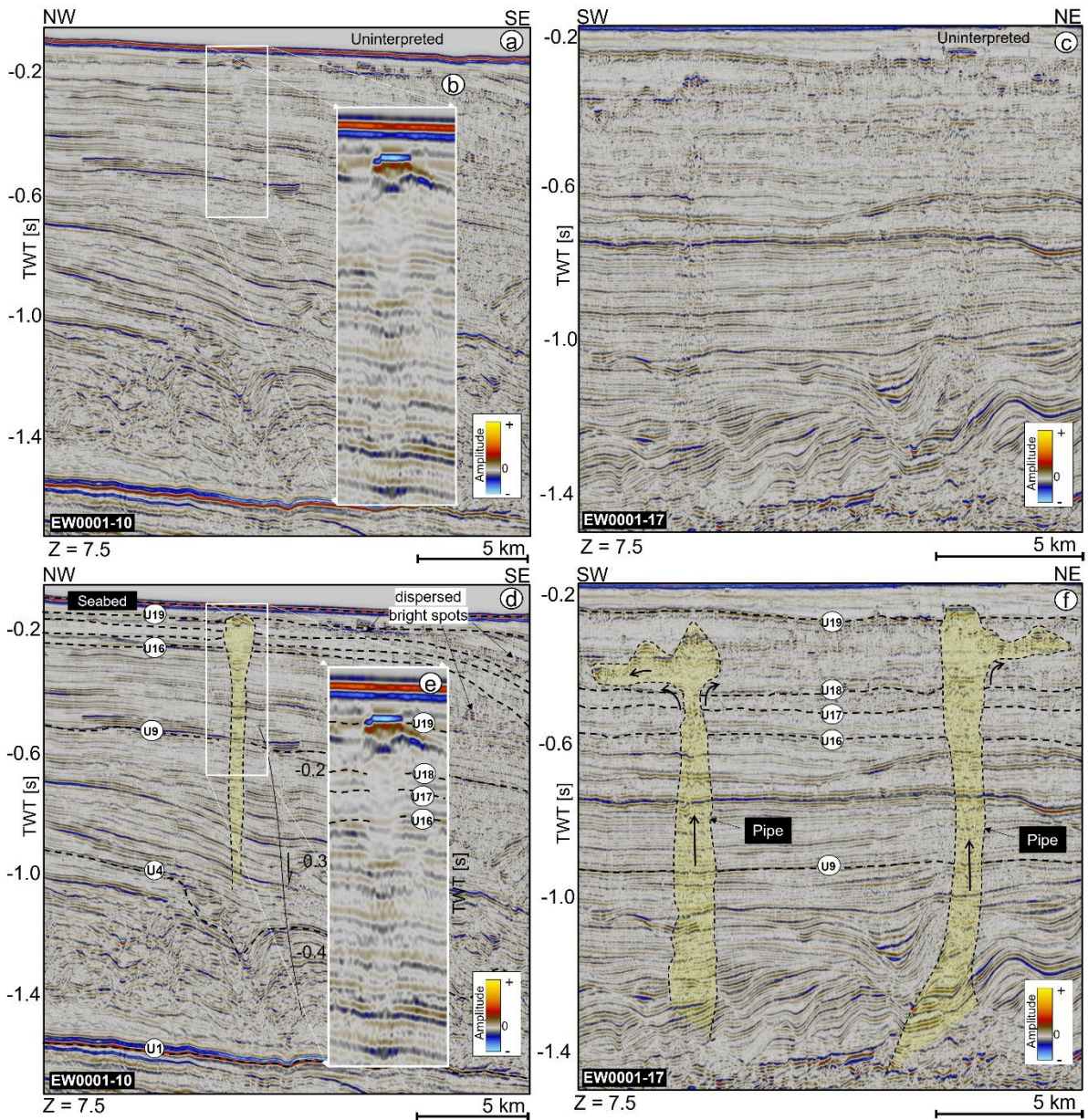


**Figure 8:** Examples of pipes from the study area. The pipes are massive vertical to sub-vertical structures that may reach up to 800 m in height and are often sourced from bottom-current circulated sediments below the U9 unconformity. (a)-(c) Uninterpreted version of the seismic sections shown in (d)-(f), (d) shows a special case of a pipe with a negative amplitude anomaly at its apex. This anomaly has a polarity that is different to the seabed reflection, and it is interpreted as fluid accumulation in the subsurface (e) zoom image of the section shown in (d), and (f) classic examples of pipes with associated lateral fluid conduits or cells at their tops.

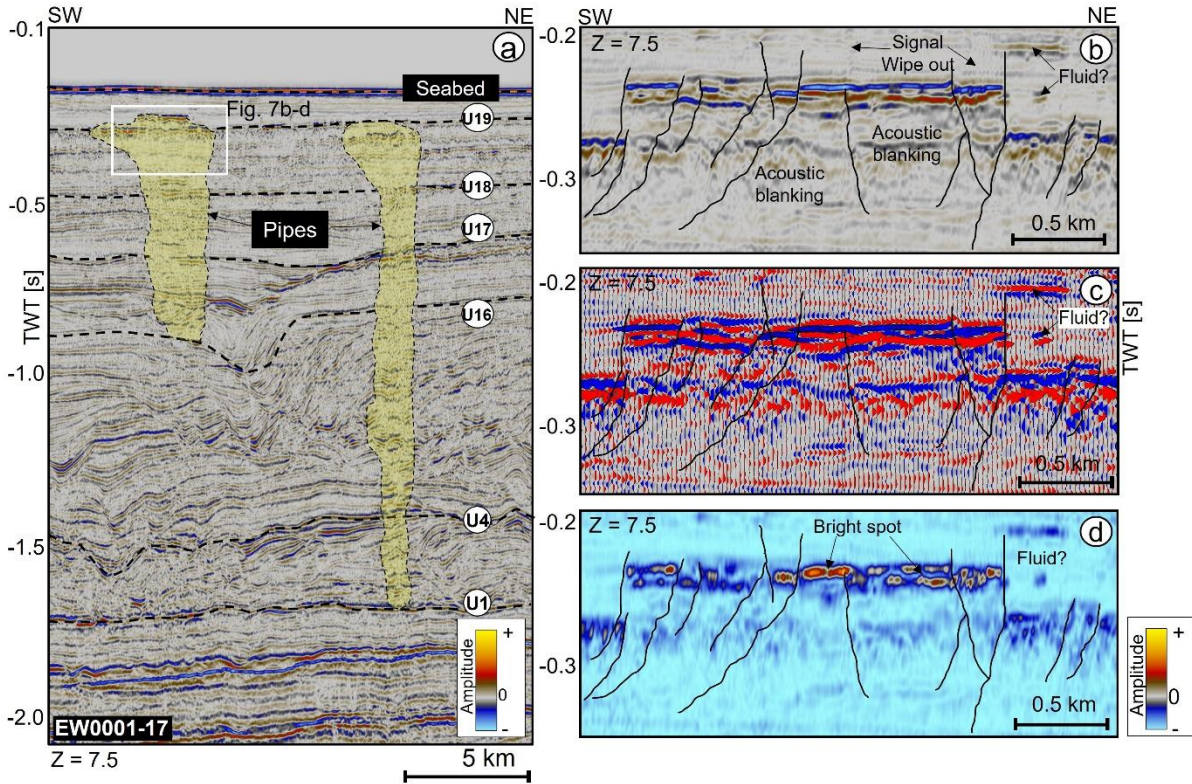


**Figure 9:** (a) Proof for the interconnection between vertical and lateral conduits in the study area. The two pipes shown here are rooted within contourite drifts or bottom current strata and are connected to lateral flow cells at their tops. (b) The enhanced reflection at the top of the pipe signify along bedding or lateral migration of fluid from areas of acoustic turbidity (Judd and Hovland, 2007; Schroot and Schüttenhelm, 2003) (c) Seismic wiggles showing flat or lateral seismic high amplitude anomalies at the top of the pipe, and (d) Envelope seismic attribute highlighting bright spots linked to fluid accumulation at the top of the pipe in (a). Note: *Uninterpreted version of the seismic profiles are provided in the supplementary data.*

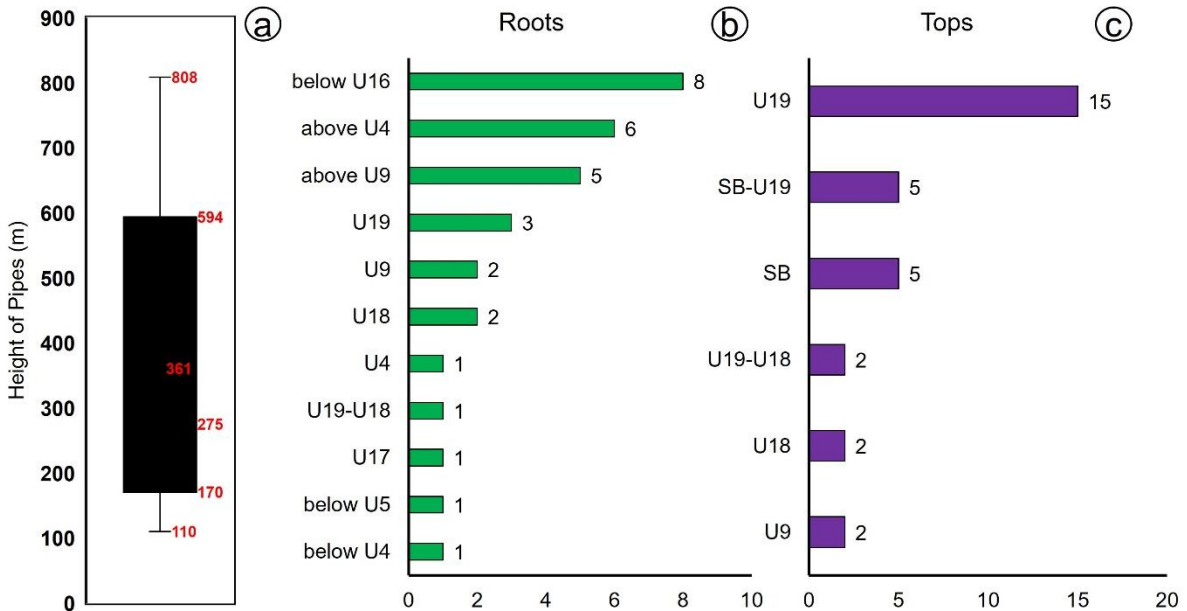


**Figure 10:** (a) Box plot showing descriptive statistics for the heights of the pipes. Heights of the pipes range between 110-808 m. Histograms showing the stratigraphic interval where the (b) root zones and (c) tops or point of termination of the pipes are found.

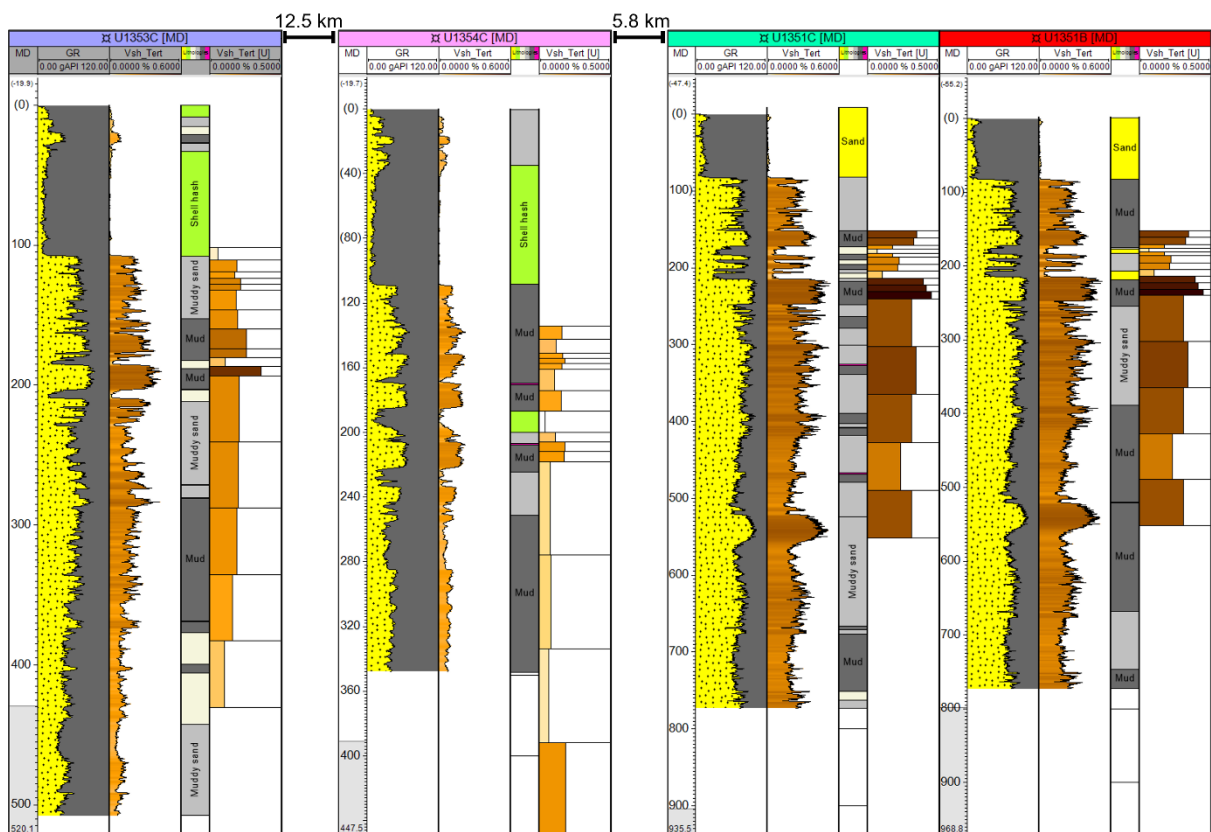


**Figure 11:** Correlation panel showing gamma ray, modeled VSh Tertiary, manually interpreted lithology of the holes based on core logs from the ODP and IODP websites (<https://www.iodp.org/resources/access-data-and-samples>) and the upscaled VSh across U1353,U1354 and U1351 used for populating the 3D geologic grids in Figure 10.

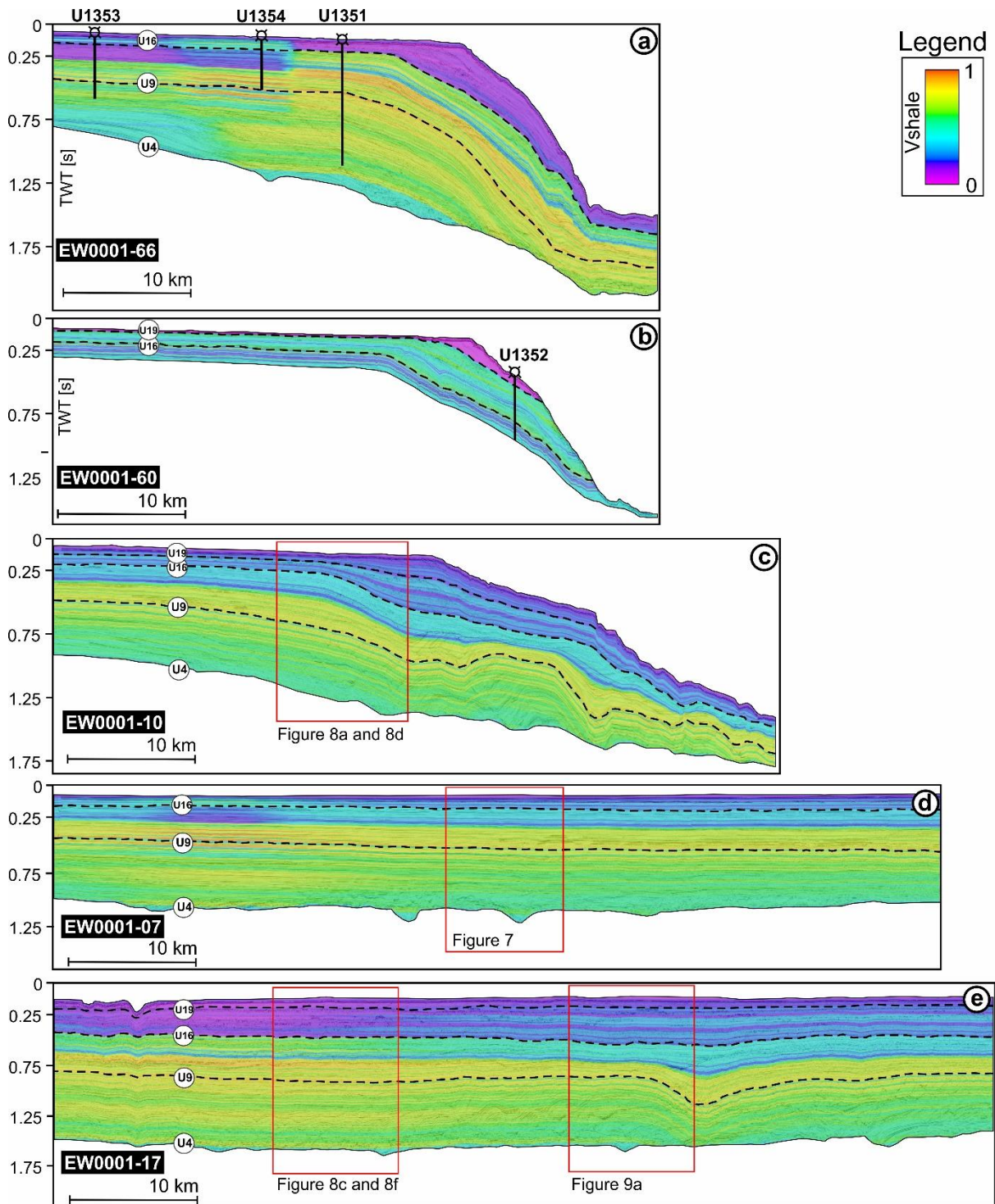


**Figure 12:** Inverted seismic profiles (a) and (b) populated with the modelled VSh (Tertiary) across the study area. Also shown is the location of the seismic profiles and pipes in Figures 6 to 8 are shown. The upper terminus of the pipes are truncated within strata of low to moderate VSh values interpreted as heterogeneous mixture of mud and sands.

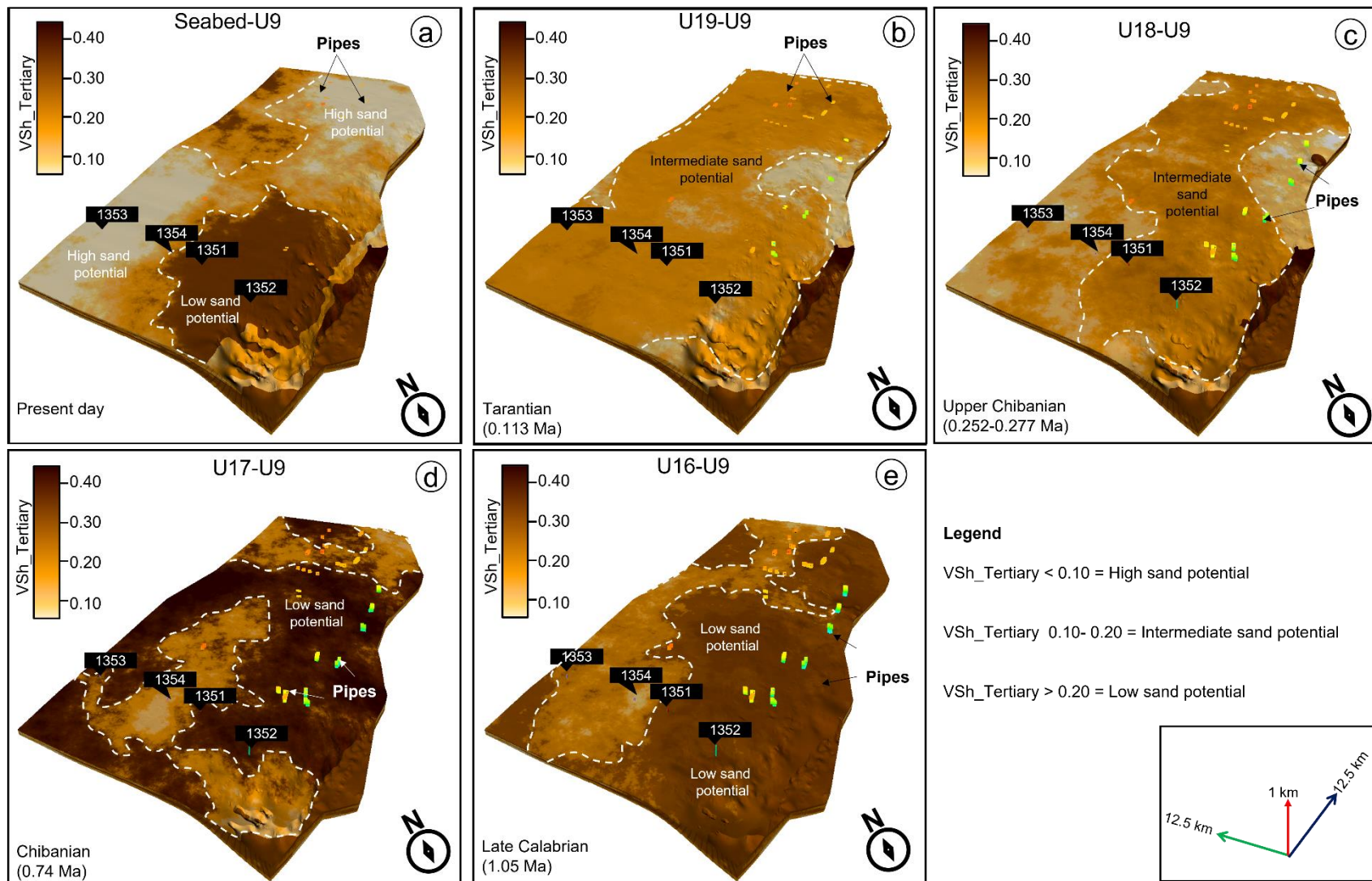


**Figure 13:** 3D evolving lithologic model based on modelled VSh Tertiary from sites U1343, U1352, and U1352 at present day from (a) Seabed to U9 (b) Tarantian (0.113 Ma) (c) Upper Chibanian (0.252-0.277 Ma) (d) Chibanian (0.74 Ma) and (e) at the latest Calabrian (1.05 Ma). Based on the Vsh (Tertiary) distribution, the study area is categorized as regions with low, intermediate and high sand potential.